Космични изследвания в България

Том 2 · София · 1979

Българска академия на науките

Address

Space Research in Bulgaria
Central Laboratory for Space Research
Bulgaria, 1000 Sofia, Blvd. Rouski 1

Адрес

Космични изследвания в България
Централна лаборатория по космични изследвания
1000 София, бул. „Руски" № 1

Издателство на Българската академия на науките

c/o, Jusautor, Sofia

629.13(05)

Коректор *Ж. Тумпарова* Техн. редактор *Л. Калинова* 9532422211
Изд. индекс 7389 Дадена за набор на 3. VIII. 1979 г. Подп. за печат на 25. VII. 1979 г. Код 19 2332-2-79
7000×1000/16 Тираж 500 Печ. коли 4,75 Изд. коли 6,16 Цена 0,76 лв.
Печатница на БАН — 1113 София, ул. „Акад. Георги Бончев" Пор. 391

Space Research in Bulgaria

Volume 2 · Sofia · 1979

Bulgarian Academy of Sciences

Contents

Содержание

BULGARIAN ACADEMY OF SCIENCES

SPACE RESEARCH IN BULGARIA, 2

Sofia · 1979

Changes in the Intensity of Solar Radiation during the Solar Eclipse of April 29, 1976

I. Apparatuses and Method of Measuring the Changes in Solar Radiation during the Eclipse of April 29, 1976

D. N. Mishev A. Y. Stoimenov, A. H. Kroumov, S. T. Kovachev, B. P. Simeonov, N. D. Pelova, T. K. Yanev

Introduction

The paper describes the apparatuses and methods worked out specially for the purpose of obtaining data about the change in the solar radiation during the eclipse of April 29, 1976.

The results were obtained on the island of Santorini in Greece and in the town of Stara Zagora in Bulgaria and are related to the slow changes in the intensity of solar radiation, in the first case, and to the rapid changes in its spectral composition at the maximum of the phase, in the second case.

Spectrometric Apparatuses

For investigating the slow changes in the intensity of the solar flux in the visible and near-infrared region of the optic spectrum we used a device, worked out by the Team on Remote Sensing at the Central Laboratory for Space Research, for measuring the spectral reflective characteristics of natural formations ISOH-010. The block diagram of the device is shown on Fig. 1. The optico-mechanical system (OMS) provides for the discretization of the visible and near-infrared region of the light spectrum by means of 11 interference filters. The average semi-width of the filters is 12 nm, with maxima at 413, 428, 443, 482, 513, 543, 596, 652, 710, 749 and 795 nm, respectively. The field of view of the optic input of the system is 15°. A phototransistor operating with accumulation of the charges has been used in the transformation of the light flux into electric signal. The phototransistor is fed by a pulse generator (PG) and a forming device (FD), which yield pulses of 2 μs durations and 450 Hz frequency of repetition. A series of pulses are obtained at the output of the FD, whose scope is proportional to the intensity of the light flux. By the peak detector (PD) this series is transformed into direct voltage measured by the pointer-type indicator I.

A multi-channel scanning spectrophotometer was designed for the purpose of investigating the rapid changes in the intensity of the solar flux. Its-block diagram is shown on Fig. 2. The input optic equipment (IOE), projects the image of the investigated object (the solar disk in this case) on the plane of the dispers.

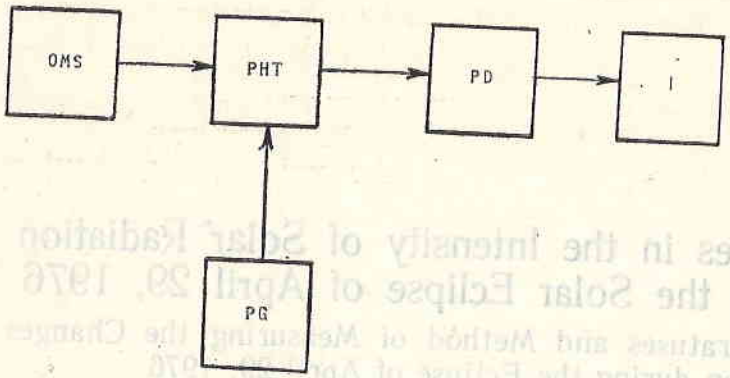

Fig. 1

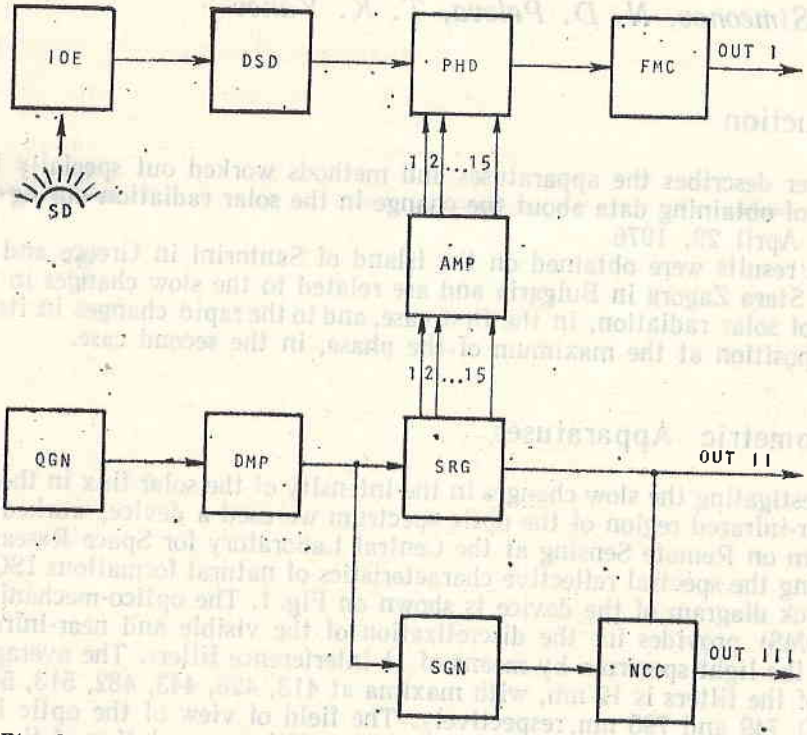

Fig. 2

ing device (DSD), at the output of which an optical spectrum is obtained with geometric dimensions suitable for the phototransducer. The dispersing device used is a volume phase hologram on diffractional grating, worked out at the Central Laboratory for Optical Registration and Processing of Information at

the Bulgarian Academy of Sciences. Its basic characteristics are: transmission coefficient — 0.3; dispersion capacity — 1000 lines/mm; optical resolution — 2 nm; dimensions — 45×45×2 mm. The use of this grating considerably simplifies the design of the spectrophotometer, reducing the loss of light and ruling out the appearance of specters of a higher order and "ghosts".

The block of the phototransducer (PHD) is a linear discrete structure of 15 phototransistors type BPY 61-III operating on a pattern of charge accumulation. The design and operation pattern provide for discretization of the output information in relation to the length of the light wave and for obtaining higher sensitivity. The total resolution for each channel, at 300 nm width of the optic spectrum, is not below 20 nm. Within the frameworks of the investigated spectral range from 450 to 750 nm, channel No. 1 records the region of 730 to 750 nm, channel No. 2 — 710 to 730 nm, etc. The mean quadratic error of the entire tract of the photoelectric conversion is below 1 per cent.

The output signal of the phototransducer has the shape of a comb function. The forming circuit (FMC) rounds off the peak of the pulse, and this permits the analogue-to-digital conversion in the first microsecond after the front.

The pattern of charge accumulation is obtained by consecutive scanning of the phototransistors with pulses obtained at the outputs of a 16-bit shift register (SRG). The sixteenth output forms a control signal "End of spectrum". In AMP the pulses from the shift register are amplified for the purpose of obtaining the necessary double amplitude of 10 V. The clock pulses for the shift register with repetition frequency of 100 Hz are produced in the quartz square-pulse generator (QGN) at a frequency of 100 KHz and demultiplied by 1000 — DMP. The quartz stabilization is necessary for the accurate observance of the scale of relative time. The same pulses also go into SGN, where strobe pulses of duration 1 μs and repetition frequency of 100 Hz are formed. The rear front of these pulses fixes the moment of measuring the double amplitude of the output signal.

Data Registration System

Underlying the system of registration for the data from the multi-channel scanning spectrophotometer (MSS) in real time is an abridged configuration of the IZOT-0310 minicomputer. The block diagram of the system and its connection with the spectrophotometer are shown on Fig. 3. Its standard part includes a central processor unit with 8K core memory, an operator's board — teletype ASR-33 control unit, and a rapid punch-tape output — DZM 180.

For the purpose of connecting the system with the multichannel scanning spectrophotometer and for converting the analogue information into digital form, a fast analogue-to-digital converter (ADC) has been used, in addition to a specially designed controller along the channel for programmed input/output transfers. The ADC is of the successive approximation type coding with 1.2 million conversions per second with 8-bit parallel binary code output.

The specialized controller receives from the spectrophotometer also control signals along the Uy bus. Its programme control from the computer is realized by a set of six specialized input-output instructions.

The automatic operation of the system in a mode of recording, the preliminary processing (compression) of the spectral information, and taking it on punched tape in real time is done under the control of a specially worked out programme. It is written in programme assembler's language and occupies only

7108 memory locations. The block diagram of the generalized algorithm of operation of the programme is shown on Fig. 4.

The synchronization of the recording process after the manual starting of the complex takes place at a signal of ES — end of the successive spectrum. Each

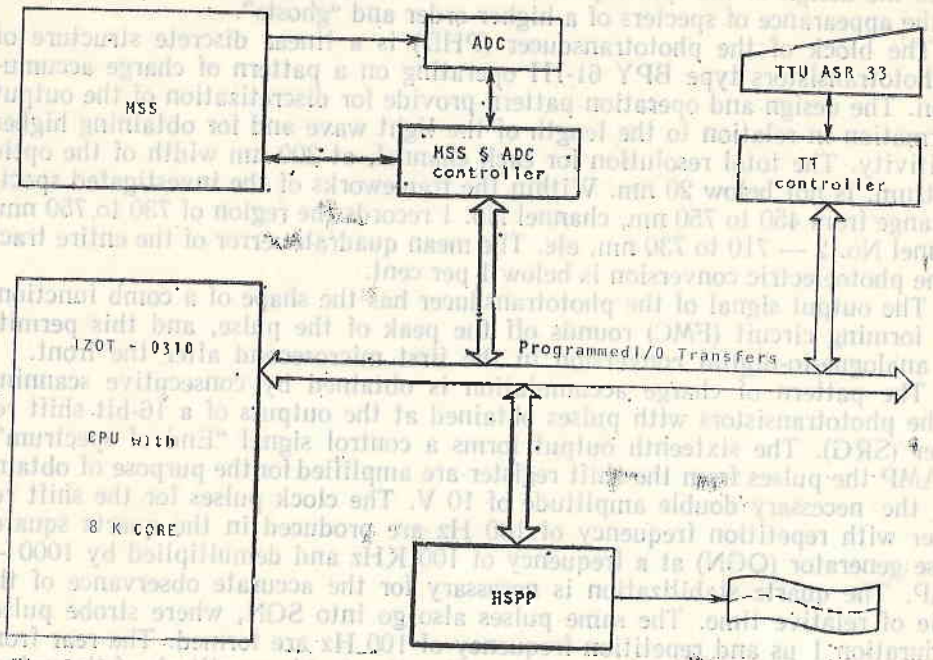

Fig. 3

successive value (point) of the currently recorded spectrum (corresponding to the light intensity for the successive band of the spectral range investigated) is compared with the value of the corresponding point from the preceding spectrum. Any difference in the values greater than the one determined in advance e. g. the mean quadratic error of the measurement and converting tract) is an indication for recording and for taking on punched tape the spectral information for the entire incoming spectrum.

Punching of the spectral information is done at the rapid punch-tape output during the passage of the even spectra and continues during the recording of the subsequent (odd) spectrum. This makes it possible to put the data on punched tape without any need to change the reel during the entire measurement. Parallel with that, each different spectrum is memorized also in the computer memory, together with its serial number (a maximum of 375 full spectra), thereby duplicating the information punched for the sake of raising the reliability of the system of recording.

Under this mode of operation the aggregate of hardware and software possesses the following major characteristics:

— Time resolution: 160 spectra/ms at 160 ms/channel;
— Number of spectra obtained: 6.25 spectra/s, or 375 spectra/min;
— Number of spectra recorded: 3.125 spectra/s, or 187.5 spectra/min;
— Number of spectra recorded; in the operative storage of the computer — 375 consecutive differing spectra; on punched tape — practically unlimited number;

— Period of uninterrupted recording: practically over 4 hours.

The programme supervises the correct operation of the system during the experiment, analysing the state of the flags of the control device for connection between the spectrophotometer and the computer and the number of consecu-

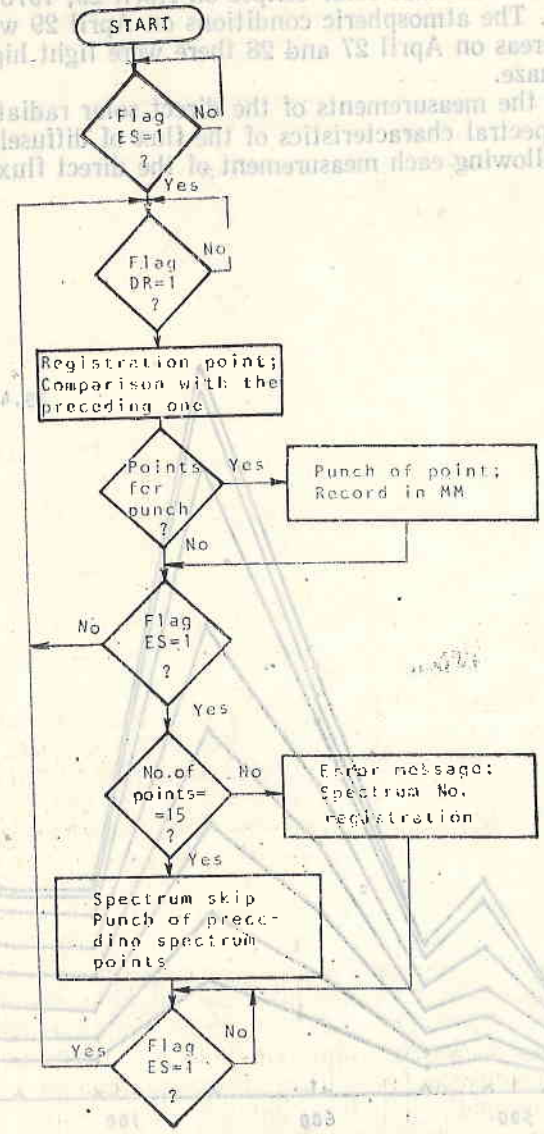

Fig. 4

tively entering points of the spectrum. In case of an accidental error, indication is given at the operator's board (bell-ring) and the number of this spectrum is memorized in a particular region of the storage. A constantly recurring error requires the intervention of the operator. The cycle of the programme is infinite and it can be stopped manually from the operator's board.

Conditions of Measurement and Results

According to preliminary instructions, the measurements on the island of Santorini in Greece were carried out at 15-min intervals, the duration of each measurement (in the 11 spectral ranges) being not longer than 2 min. The measurements embrace the interval from 10:00 h Eastern European time to 15:00 h both on the day of the total annular solar eclipse on April 29, 1976, and on the days of April 27 and 28. The atmospheric conditions on April 29 were ideal for such investigations, whereas on April 27 and 28 there were light high-altitude clouds and atmospheric haze.

In addition to the measurements of the direct solar radiation, records were taken also of the spectral characteristics of the flux of diffusely scattered light. For the purpose, following each measurement of the direct flux, the direction of

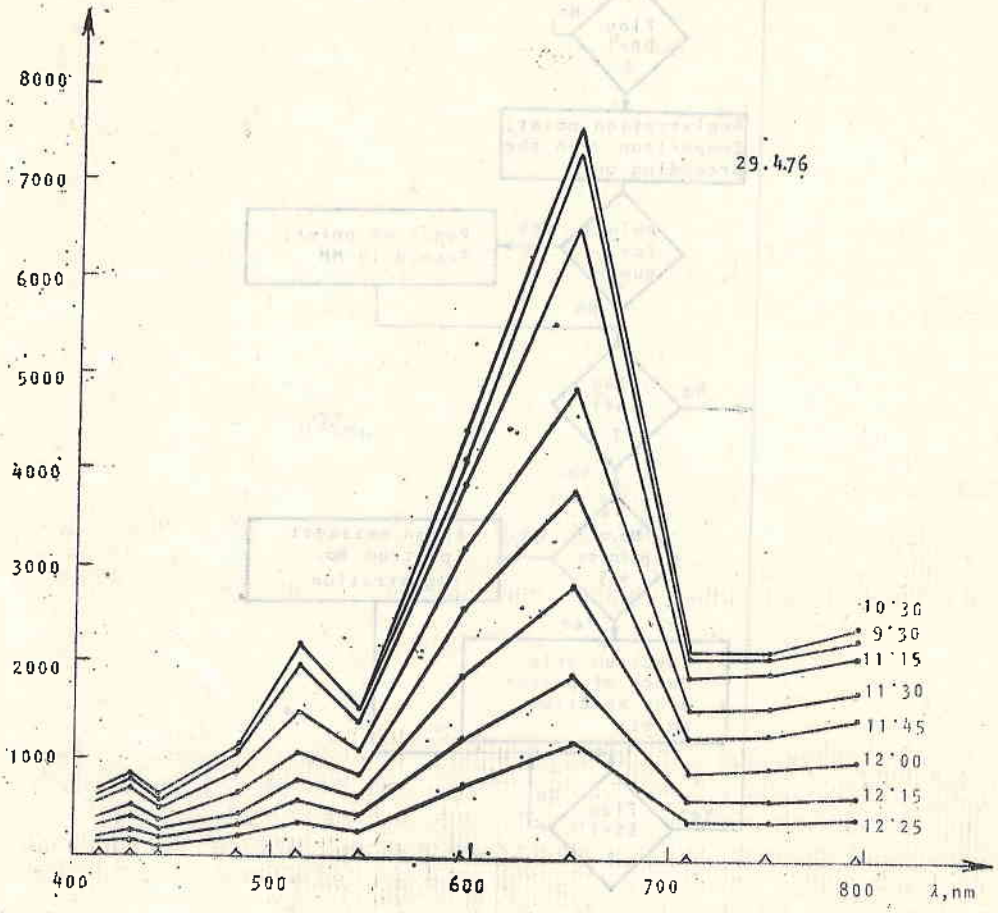

Fig. 5

measurement was changed at an angle of 180° in the horizontal plane, preserving the angle in the vertical plane. Neutral filters were used at the input of the optical equipment due to the high intensity of the light flux upon direct orientation toward the Sun. The device was oriented immediately before each measurement.

In order to make a relative quantitative evaluation of the measurement of the intensity of the light fluxes at the different phases of the eclipse, the va-

lues of the quantities measured upon using neutral filters have been reduced to the values recorded without them in relative units. The intensity of a flux causing the maximum deflection of the indicator without the use of filter has been accepted as having 100 relative units.

All data obtained from the observations have been tabulated and prepared for further processing. Figure 5 shows the change in the intensity of the direct light flux depending on the time for the eleven spectral ranges investigated.

The measurements in Stara Zagora of the intensity of the direct light flux during the partial (79%) annular solar eclipse were carried out in the interval of 11:00 to 14:00 with average duration of 4 min and 10 successive measurements. Four of them were concentrated around the phase of the eclipse, and the measurement during the phase continued for 10 min. Slight haze appeared during some of the measurements, and one of them reacted to the trail of exhaust gases left by some plane along the path of the light flux. The measurements envisaged at the same time intervals during the following day, April 30, could not be carried out on account of dense clouds and rain. The direction of the input optic device of the multi-channel spectrophotometer was done by hand prior to each optic or electronic measurement.

The data from the measurements were recorded on punched tape in real time in eight-bit binary code. During the investigations, the automatic control of the veracity of the information recorded and the subsequent comparison of the punched tape from the direct recording and the dump of the region for data in the memory after each recording, all showed the perfect working condition of the apparatuses during their operation.

To provide visual presentation for the great volume of data obtained, the results from the punched tapes were printed in tabular form, and the values of the intensity depending on the time were tabulated for each channel investigated.

Conclusions

In the course of the investigation of the changes in the intensity of the solar radiation during the solar eclipse, measurements were taken of both the main and the rapid changes in the solar flux in the visible and near-infrared region of the spectrum. The data obtained were processed by UZOT-0310 minicomputer, and the results of that processing are contained in the article entitled "Statistical Analysis of the Change in Solar Radiation during the Eclipse of April 29, 1976" which is published in the present issue.

The method worked out and the apparatuses designed provide for universal application and may be used in a number of studies — daily and seasonal ones — of the dynamics of the changes in solar radiation, of the diffuse scatter of light in the atmosphere, and in other studies.

The results obtained and the experience accumulated point to a number of changes and improvements which may be introduced in the design and operation of the complex. A portable variant of the system is to be designed, involving the utilization of microprocessor modules and the introduction of new methods of compression and of preliminary processing of the data obtained in real time.

Изменение интенсивности солнечной радиации во время солнечного затмения 29 апреля 1976 г.

I. Аппаратура и метод для измерения изменений солнечной радиации во время солнечного затмения 29 апреля 1976 г.

Д. Н. Мишев, А. Й. Стоименов, А. Х. Крумов, С. Т. Ковачев, Б. П. Симеонов, Н. Д. Пелова, Т. К. Янев

(Р е з ю м е)

В работе описаны эксперименты, проведенные в Греции — на острове Санторини и в Болгарии — в гор. Стара-Загора для исследования солнечной радиации во время солнечного затмения 29 апреля 1976 г. Дано подробное описание использованной спектральной аппаратуры и системы регистрации быстрых спектров на базе мини-ЭВМ, их параметры и действие. Приведены условия проведения эксперимента и дана предварительная обработка полученных результатов.

BULGARIAN ACADEMY OF SCIENCES

SPACE RESEARCH IN BULGARIA, 2

Sofia · 1979

Changes in the Intensity of Solar Radiation during the Solar Eclipse of April 29, 1976

II. Statistical Analysis of the Changes in Solar Radiation during the Eclipse of April 29, 1976

T. K. Yanev, N. D. Pelova, A. Y. Stoimenov, A. H. Kroumov, S. T. Kovachev, D. N. Mishev

A statistical analysis has been made of the data obtained about the variations in solar radiation during the eclipse of April 29, 1976. The results were obtained on the island of Santorini in Greece and in the town of Stara Zagora in Bulgaria [1].

In the first case the information obtained was about the slow changes in the intensity of solar radiation, while in the second case it was about the rapid changes in the spectral composition of solar radiation, mainly at the maximum of the eclipse phase.

The Island of Santorini

The data about the change of $I(t)$ were obtained during relatively long intervals of 10 to 30 min. The average value of $I(t)$ for an interval of 1-2 s was established at each measurement [2].

The analysis of the data on $I(t)$ shows that the ratio of two neighbouring spectra in time is in many cases close to constant as regards the parameter wavelength and with t fixed, i. e. that two neighbouring spectra are in an approximately multiplicative ratio. This ratio should have been accurately multiplicative if the Sun was a fully homogeneous source of radiation and if the tract of propagation and registration did not contain any noise. Of course, the size of this constant (it is a constant at fixed time and parameter — wavelength) changes depending on time, both on account of the change in the inclination of the Sun and on account of the covering of the Sun's disk in the course of the eclipse.

Table 1 contains the values of the ratios

$$\beta_{j,j+1}^{(\lambda)} = I(\lambda, t_j)\, I(\lambda, t_{j+1})$$

of the neighbouring in time recorded spectra of $I(t, \lambda)$. The variation coefficient V_β of the series obtained of $\beta_{j,j+1}$ has also been calculated. Under conditions

Table 1

Ratios $\beta_{jj+1}=I(\lambda, t_j)/I(\lambda, t_{j+1})$

No.	Hour	λ_1	λ_2	λ_3	λ_4	λ_5	λ_6	λ_7	λ_8	λ_9	λ_{10}	λ_{11}	V
1	09^{30}, 10^{00}	0.889	0.881	0.880	0.904	0.774	0.862	0.994	0.957	0.981	0.985	0.988	0.076
2	10^{00}, 10^{30}	1.046	1.067	1.056	1.091	1.300	1.161	0.977	1.015	1.000	1.000	0.983	0.089
3	10^{30}, 10^{45}	1.000	0.990	1.005	0.981	0.758	0.980	1.000	1.000	1.000	0.989	1.017	0.075
4	10^{45}, 10^{56}	0.963	0.971	0.968	0.987	1.265	1.000	1.006	1.036	1.017	1.027	1.012	0.139
5	10^{56}, 11^{00}	1.014	1.013	1.003	1.032	1.089	1.069	1.043	1.059	1.048	1.052	1.047	0.025
6	11^{00}, 11^{15}	1.062	1.055	1.058	1.046	1.036	1.021	1.028	1.052	1.047	1.031	1.049	0.013
7	11^{15}, 11^{30}	1.170	1.182	1.220	1.206	1.349	1.275	1.217	1.344	1.231	1.236	1.223	0.047
8	11^{30}, 11^{45}	1.250	1.235	1.261	1.233	1.341	1.297	1.218	1.264	1.232	1.235	1.224	0.029
9	11^{45}, 12^{00}	1.414	1.429	1.426	1.664	1.387	1.346	1.393	1.369	1.389	1.336	1.416	0.062
10	12^{00}, 12^{15}	1.603	1.609	1.593	1.311	1.448	1.527	1.566	1.486	1.513	1.528	1.492	0.059
11	12^{15}, 12^{25}	1.628	1.611	—	1.614	1.616	1.606	1.650	1.616	1.608	1.632	1.610	0.008
12	12^{25}, 12^{35}	1.137	1.277	—	1.448	0.740	0.792	1.796	1.860	1.492	1.488	1.608	0.279
13	12^{35}, 12^{42}	2.426	2.593	2.075	1.838	2.440	2.991	1.825	1.680	1.734	1.691	1.656	0.218
14	12^{42}, 12^{47}	1.042	1.034	1.024	1.072	1.000	0.955	0.953	0.969	0.947	0.955	0.951	0.045
15	12^{47}, 13^{00}	0.454	0.169	0.197	0.171	0.242	0.208	0.334	0.349	0.364	0.364	0.367	0.334
16	13^{00}, 13^{15}	1.206	1.136	1.091	1.304	1.397	1.296	0.564	0.536	0.634	0.640	0.601	0.367
17	13^{15}, 13^{30}	0.594	0.597	0.597	0.614	0.673	0.639	0.634	0.687	0.642	0.646	0.642	0.048
18	13^{30}, 13^{45}	0.753	0.754	0.744	0.763	0.786	0.791	0.756	0.793	0.816	0.819	0.814	0.036
19	13^{45}, 14^{00}	0.798	0.812	0.815	0.837	0.808	0.836	0.852	0.820	0.856	0.831	0.845	0.023
20	14^{00}, 14^{15}	0.918	0.925	0.904	0.919	0.880	0.897	0.909	0.862	0.874	0.909	0.875	0.013
21	14^{15}, 14^{30}	0.967	0.961	0.954	0.961	0.956	0.952	0.955	0.959	0.974	0.944	0.962	0.008
22	14^{30}, 14^{36}	0.992	1.019	0.994	1.014	1.046	1.033	1.000	1.022	1.015	1.000	1.000	0.017
23	14^{36}, 14^{45}	1.030	0.988	1.017	1.007	1.000	1.000	1.008	1.020	1.000	1.016	1.026	0.013

of completely homogeneous source of light and of undisturbed transmission-reception tract, the variation coefficient must be equal to zero, regardless of the movement of the Sun's disk and of its being covered by the Moon's disk during the eclipse. These properties of V_β make it suitable for an integral assessment of both phenomena, namely, inhomogeneity of the Sun and noise in the transmission-reception tract.

Table 1 shows that the variation coefficients related to the phase of the eclipse are the biggest and, at the same time, they are by one order bigger than the other variation coefficients.

Stara Zagora

The main object of the investigation in the recording of the solar eclipse in Stara Zagora were the rapid transitional processes in the intensity $I(t)$ of the solar radiation. Presented in this article are the processed data from the "phase" of the eclipse [2].

The dynamics of $I(t)$ is characterized by its first derivative in time. In view of the fact that the data are in a discrete form and the interval of discretization is constant, an evaluation of the size of the first derivative may be obtained from the neighbouring differences $\Delta I_{j,\,j+1}=I_j-I_{j+1}$, which have been further used in investigating the changes of $I(t)$.

The analysis of the neighbouring differences $\Delta_{j,\,j+1}$ has shown the existence of strong grouping (over 95%) for all channels in three intervals: for $\Delta_{j,\,j+1}$ $=-2$, 0 and 2 relative units (one such unit is equal to 40 mV). This does not make it possible to apply correctly the χ^2-criterion for evaluating the degree of proximity with normal distribution. Nevertheless, on the basis of considerations for many, mutually independent, random and equal factors (each one of them with a small contribution to the total dispersion) affecting the formation of $\Delta I_{j,\,j+1}$, it may be assumed that in these intervals the distribution will be close to the normal one. Under this assumption a check was made with the r-criterion for gross deviations from $\Delta\bar{I}$ [3]:

$$r=\frac{|\Delta I\max,\ \min-\Delta\bar{I}|}{S}, \qquad S=\sqrt{\frac{\sum_{(i)}(\Delta I_{j,j+1}-\bar{I})^2}{n-1}}.$$

All differences $\Delta I\geqslant 4$ relative units proved to be non-inherent to the assumed normal distribution in the above three untervals. That is why these differences are further on treated as bearers of the basic information about the dynamics of the transitional processes ΔI and are called *supraliminal differences.*

The supraliminal differences for all pairs of channels were investigated by linear correlation and regression analysis (single correlation), provided in a given pair of channels in the course of the eclipse phase there apperaed supraliminal differences of more than 4 times and simultaneously in both channels of the examined pair of channels. The intensity in the channel bearing a smaller number was accepted as the x argument. The coefficient of linear correlation r, the regression coefficients of the model, and Fisher's F-criterion for adequacy of the linear model were calculated.

The analysis indicates that the correlation between the supraliminal differences is comparatively poor, with the exception of the following pairs of channels: 6-11, 6-12, 8-13, and 9-13, for which $r>0.70$ and $F>F_\tau$ at a confidence level of $p<0.05$.

Table 2

Supraliminal Differences for Groups of Three Channels for Which the Common Coefficient of Correlation is $R>0.70$

Channel	Sp.		
	1269	1290	1639
VI	—4	— 4	—2
XI	—6	8	6
XII	4	—10	4

Channel	Sp.				
	783	832	1009	1365	1394
VIII	—16	8	—8	—44	44
IX	— 4	4	4	116	—116
XIII	- - 6	4	—8	—24	24

Channel	Sp.									
	411	537	783	832	1072	1269	1333	1365	1394	1444
VIII	4	8	—16	8	—8	—8	— 4	—44	44	4
XII	4	12	— 6	12	—8	4	—4	26	—26	26
XIII	6	8	— 6	4	4	—6	—4	—24	24	—26

Channel	Sp.			
	783	832	1365	1444
VIII	—16	8	—44	4
XII	— 6	12	26	26
XIV	— 6	4	—32	—34

Channel	Sp.				
	301	783	832	1565	1394
IX	116	—4	4	166	—166
XII	—24	—6	12	24	— 26
XIII	4	—6	4	—24	24

Channel	Sp.							
	301	416	783	832	1360	1365	1444	1454
XII	—24	4	—6	12	—6	26	26	—28
XIII	4	6	—6	4	—6	—24	—26	24
XIV	6	4	—6	4	—4	—32	—34	8

Channel	Sp.
	1269
VI	—4
XII	4
XIII	—6

One characteristic feature is that the synchronous appearance of supraliminal differences in a given pair of channels is divided by irregular and long time intervals.

Table 2 contains the combinations of each three out of all channels in which there is simultaneous appearance of supraliminal differences connected with a single correlation coefficient $r>0.70$.

Conclusion

The principal results from the analysis of the data about the solar eclipse of April 29, 1976, may be formulated as follows:

Island of Santorini

Since on the island of Santorini the eclipse was annular during the phase (96%) and the observations of the Sun's disk were carried out in clear weather, it may

be assumed that the large values of the variation coefficient V_β during the phase are due in the first place to inhomogeneity in the visible part of the Sun (about 4 per cent of the full disk). The contribution of the error of the measurement device for raising the variation coefficient is inessential because the maximum error of the apparatus used is about 1 per cent.

The variation coefficient is independent of the constant of the neutral filters. That is why, neutral filters of unknown constant may be used for obtaining primary information about the intensity of the solar radiation (the constant is cancelled in the expression for V_β).

The Town of Stara Zagora

The distribution of the neighbouring differences $\Delta I_{j,\,j+1}$ in all channels is expressed unimodally by an arithmetical mean almost equal to zero and by incidental supraliminal differences of various magnitude. This shows that there is no predominant manner in which the rapid transitional processes $I(t)$ take place during the observed phase of the eclipse.

The linear correlation among the values of the supraliminal differences is poor, with the exception of several pairs of channels for which $r>0.70$ and $F>F_T$ at a confidence level of $p<0.05$.

In channels 8 to 13 there exists a marked tendency toward simultaneous appearance of the supraliminal differences [2].

References

1. Mishev, D. N., A. I. Stoimenov, A. H. Kroumov, S. T. Kovachev, B. P. Simeonov, N. D. Pelova, T. K. Yanev. — Space Res. in Bulg., 2, 3.
2. Отчет Р — 5/1. Подготовка, провеждане и резултати от изследването на Слънчевото затъмнение на 29 април 1976 год. — ЦЛКИ при БАН, София, 1976 г.
3. Смирнов, Н. В., И. В. Дунин-Барковский. Курс теории вероятностей и математической статистики. М., 1965 г.

Изменение интенсивности солнечной радиации во время солнечного затмения 29 апреля 1976 г.

II. Статистический анализ изменения солнечной радиации во время солнечного затмения 29 апреля 1976 г.

Т. К. Янев, Н. Д. Пелова, А. Й. Стоименов, А. Х. Крумов, С. Т. Ковачев, Д. Н. Мишев

(Резюме)

В работе проведен статистический анализ данных об изменении солнечной радиации I во время солнечной затмения 29. IV. 1976 г. Данные снимались на острове Санторини, Греция и гор. Ст.-Загора, Болгария.

В первом случае снималась информация о медленных изменениях солнечной радиации, а во втором — быстрые изменения по спектру, в основном во время максимума фазы затмения.

Анализ медленных изменений проводился с исследованием отношений I для соседних во времени спектров, а быстрые изменения — разностями соседних спектров.

Основные результаты проведенного анализа:

— наблюдаются значительные по амплитуде медленные изменения интенсивности солнечной радиации во время фазы затмения, которые можно объяснить негомогенностью видимой во время фазы части солнечного диска.

— быстрые изменения (переходные процессы) не сопровождаются каким-либо превалирующим видом закономерности во времени.

BULGARIAN ACADEMY OF SCIENCES

SPACE RESEARCH IN BULGARIA, 2

Sofia · 1979

Ion and Electron Analysis in Retarding Electric Field for Ionospheric Studies Performed with the Intercosmos-8 Satellite

K. I. Gringaus, G. L. Gdalevich, V. F. Gubskiy, K. B. Serafimov, S. K. Chapkunov

Introduction

The Intercosmos-8 satellite was launched on December 1, 1972. Experiments on this satellite were a continuation of the ionospheric studies initiated by the Intercosmos-2 satellite [1-4] and by the geophysical rockets Vertical-1 and Vertical-2.

Specialists from Bulgaria, the German Democratic Republic, USSR and Czechoslovakia took part in the study.

The initial orbital parameters of Intercosmos-8 were the following: apogee — 679 km, perigee — 214 km, inclination — 71°, and period — 93.2 mm.

The following measurements were carried out:

1. Positive ion density.
2. Electron temperature.
3. Electron density and temperature.
4. Intergal electron density between the satellite and the ground-based radio-receiving stations.
5. Electron fluxes with 40 keV and protons with 1 MeV of energy.

The following scientific equipment was installed on the satellite:

— Sensors of the instruments for ionospheric parameter measurements; semiconducting and gas-discharge counters for high-energy electrons and protons (USSR).

— Instrument for plasma parameter measurements with the help of ion traps and Langmuir probe (Bulgaria).

— "Mayak" radio-emitter and intermediate device for the registration of the Langmuir probe data in the satellite memory (GDR).

— Instrument for measurements of electron temperature with a high-frequency probe (Czechoslovakia).

Specialists from Bulgaria, the German Democratic Republic and Czechoslovakia took part in the technological and launch tests of the above items of equipment. They also took part in the satellite launch.

The experimental data obtained as a result of the measurements carried out on the satellite with the scientific equipment were processed as follows: from the ion traps — in Bulgaria and in the USSR; from the Langmuir probe — in Bulgaria and in the USSR, from the high-frequency probe in Czechoslovakia and in the USSR.

Information on the Soviet-Bulgarian Probe Experiment with Intercosmos-8

The choice was a satellite with chemical battery, for carrying out the experiments listed above. The purpose was to reduce to the minimum the medium deformation caused by the satellite during the probe measurements. The currents of the solar batteries were apt to generate magnetic fields, despite the precautions taken. Their influence on the measurements of the cold ionospheric plasma local parameters is difficult to be accounted for.

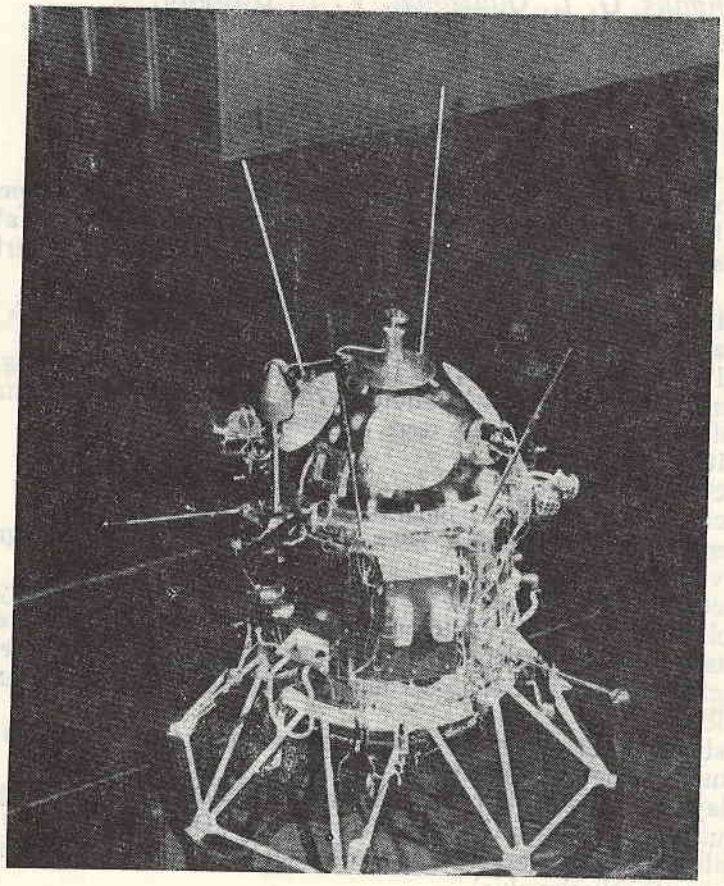

Fig. 1. General view of the Intercosmos-8 satellite

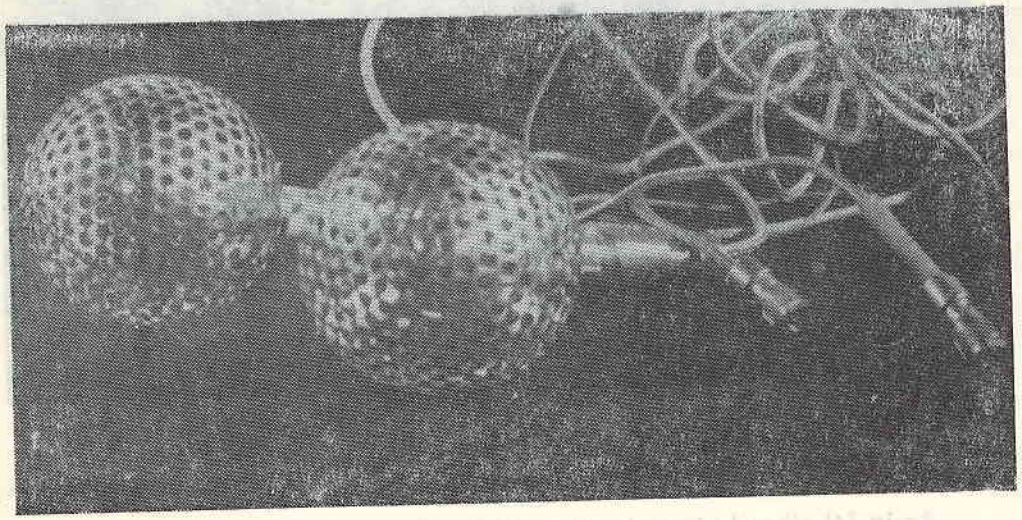

Fig. 2. View of the Intercosmos-8 ion traps

The satellite did not have an orientation system, but it was provided with equipment ensuring the determination of its direction with respect to the magnetic field and the Sun (Fig. 1). As the satellite was not oriented, the ion traps were spherical in shape, which ensured the minimum dependence of the measurement results on the probe orientation. The iron traps were mounted on booms diametrally opposed to one another, so that at any moment one of them could be out of the rarefied zone which was formed in the direction opposite to the satellite velocity vector. The Langmuir probe was mounted on the central cross-section plane of the satellite, perpendicular to the two traps.

The spherical ion traps are the first instruments with which the successful ionospheric study by direct probe techniques had begun and the first distribution of the ionospheric charged particle concentrations had been obtained [6]. Since then, spherical ion traps have been applied on a number of occasions for ionospheric measurements in the Soviet Union and in other countries.

The traps used on Intercosmos-8 (Fig. 2) were 60 mm in diameter and were mounted on booms 500 mm in length, so as to be out of the layer with the bulk electric charge which surrounded the satellite. The collector of each trap was 20 mm in diameter and was enveloped in an anti-photoelectronic grid 26 mm in diameter. A potential of — 100 V with respect to the satellite body was applied to the grids. Isolated voltage of —80 V with respect to the amplifier inputs (see [5]) was applied to the collectors for full ion collection in the internal space of the traps.

A linearly changing voltage, varying from —5 V to +15 V for 6 s with respect to the satellite, was applied to the outer grids of the traps. Much like in the case described in [1], this voltage was applied in turns to the outer envelopes.

The currents measured were commutated in turns to the input of the same amplifier [7], in order to reduce the indeterminateness introduced by the drift of the different DC amplifiers, and also to reduce the energy source, the weight and the number of the telemetric channels necessary for data broadcasting.

The determination of the positive ion density was accomplished by the technique suggested in [6], i. e. along the slope of the volt-ampere curve.

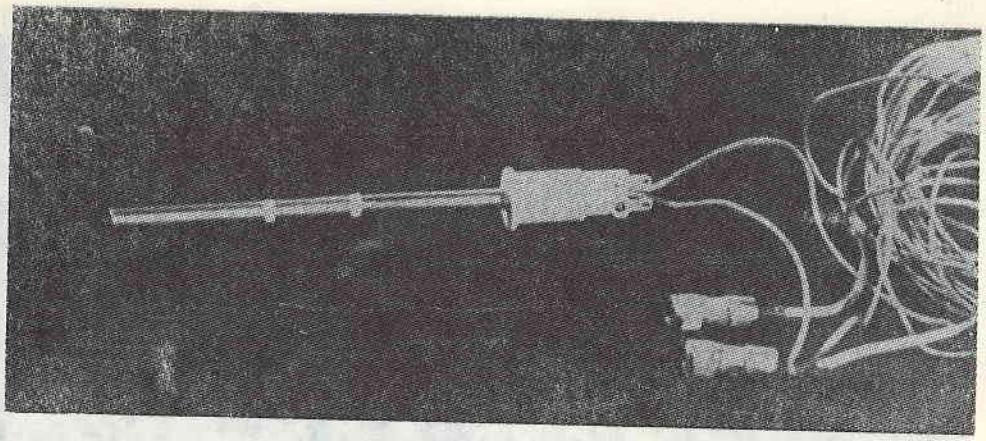

Fig. 3. View of the Intercosmos-8 Langmuir probe

As in [4], the electron density and the temperature were measured by the method of the Langmuir probe. Only one cylindrical Langmuir probe was mounted on the Intercosmos-8 satellite (Fig. 3). The probe was detached from the satellite body by a boom 500 mm long.

The probe (Fig. 3) was 6 mm in diameter and 20 mm long, and it was positioned between two protective sections. The overall length of the probe and of the protective sections was 110 mm. The probe voltage varied from — 1V to +4 V in 1 s.

Unlike in the case of the Intercosmos-2 experiment, the present measurements of the electron temperature and density, made with the Langmuir probe were carried out not only during the direct radiotelemetric connection with the ground-based receiving stations, i. e. in the zones of the direct visibility of the satellite, but also out of the limits of these stations.

By means of the satellite memory device the Langmuir probe operated in memory-regime, and this made it possible to retain the measurement results during the full satellite turn around the Earth, followed by informational emission effected by the telemetric communication line.

The ion trap data were also recorded during the satellite flight out of the visibility zone of the receiving radiotelemetric station.

Brief Characteristics of the Recorded Information

The operation of the satellite equipment continued for almost two months, and during that time it was possible to have a number of direct radio-communication seances, as well as reproduction of the information kept by the memory device during the full satellite turns of the Earth.

The results from the probe measurements of the local parameters n_e (or n_i) close to the satellite, together with the data from the ground observations on coherent radiowaves, can be used for the determination of the vertical distribution N (h) up to the satellite altitudes. Records of the volt-ampere characteristics are given below.

The records of the telemetric control on the saw-tooth voltage applied to the trap envelopes, as well as the volt-ampere characteristics of the iron traps,

are shown on Fig. 4. During the first six seconds we recorded the collector current of the trap, to the outer envelope of which a linearly changing voltage was applied, and the envelope of the other trap was simultaneously provided with a potential of —5V with respect to the satellite body. The second trap operated during the following 6 seconds, and the outer grid of the first trap was provided with a potential of —5 V. In this manner we can see both spherical traps in operation on the same record, and this facilitates the processing of the results of the experiment.

Figure 5 shows records of the telemetric control of the saw-tooth voltage which is applied to the collector and of the protective electrodes of the Langmuir cylindrical probe, as well as a record of the volt-ampere characteristics of this probe under conditions of direct data transmission.

Records of the telemetric control of the linearly changing voltage, and volt-ampere characteristics of the Langmuir probe are shown in memory regime on Fig. 6. The saw-tooth voltage generator [5] is controlled under these conditions

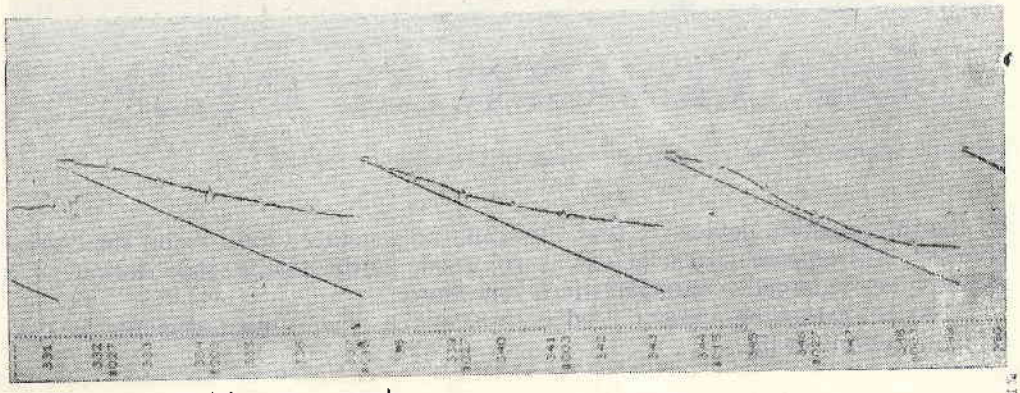

Fig. 4. Ion traps telemetric records

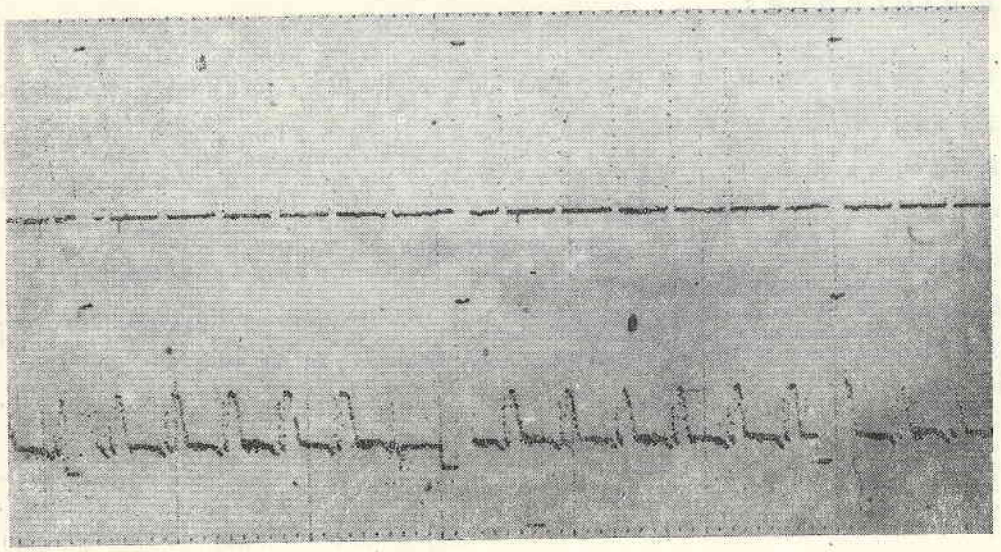

Fig. 5. Langmuir probe records in real time telemetry

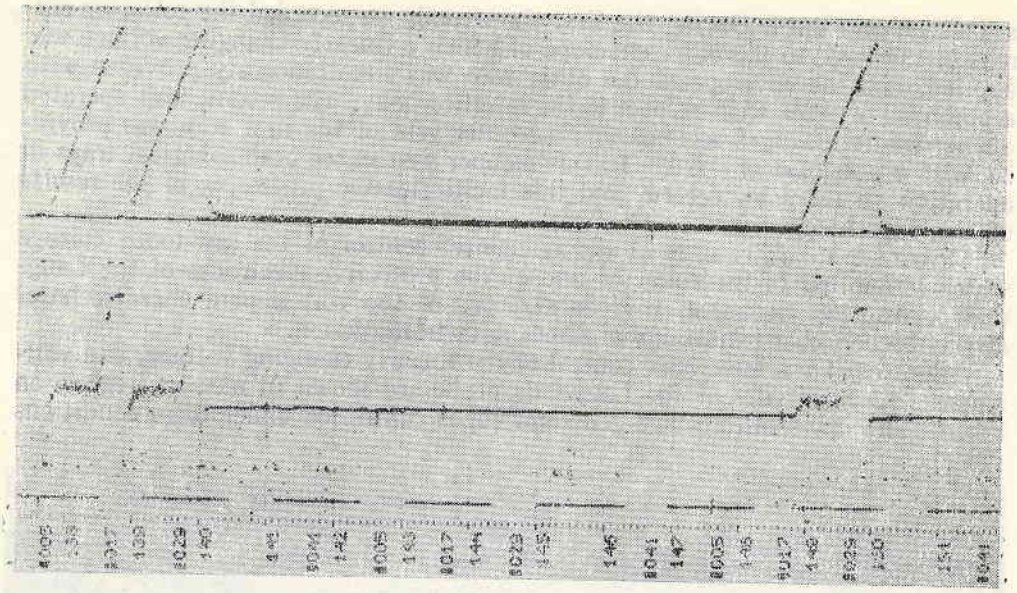

Fig. 6. Langmuir probe telemetric records in the memory regime

by the intermediate device, so that the scanning generated for 1 s and the corresponding volt-ampere characteristic is recorded, while during the following 8 seconds the "enlarged" characteristic is reproduced.

The Bulgarian equipment used in taking the above measurements is described in detail in [5].

References

1. Грингауз, К. И., К. Б. Серафимов, К. Г. Шмеловский, Я. Шмилауер. — Косм. исследования, 11, 1, 1973.
2. Гдалевич, Г. Л., Б. Н. Горожанкин, И. С. Кутиев, Д. Т. Самарджиев, К. Б. Серафимов. — Косм. исследования, 11, 2, 1973.
3. Афонин, В. В., Г. Л. Гдалевич, К. И. Грингауз, Я. Кайнарова, Я. Шмилауер. — Косм. исследования, 11, 2, 1973.
4. Бишофф, К., Г. Л. Гдалевич, В. Ф. Губский, И. Д. Дмитриева, Г. Цимерман. — Косм. исследования, 11, 2, 1973.
5. Чапкынов, С. К., Т. Н. Иванова, М. Х. Петрунова. — Научные приборы, 5, Москва, 1974, 39—42.
6. Грингауз, К. И., В. Д. Безруких, В. Д. Озеров. — Искусственные спутники Земли, 6, АН СССР, 1961, 63.
7. Chapkunov, S. K. — Compt. rend. Acad. bulg. sci., 24, 11, 1971.

Исследование структурных параметров ионосферы методом анализа ионов и электронов в запирающем электрическом поле, проведенное при помощи ИСЗ „Интеркосмос-8“

К. И. Грингауз, Г. Л. Гдалевич, В. Ф. Губский, К. Б. Серафимов, С. К. Чапкынов

(Р е з ю м е)

Вкратце перечислены эксперименты и реализирующие их аппаратуры, включенных в состав спутника „Интеркосмос-8“.

Рассмотрены зондовые эксперименты для исследования электронной концентрации и электронной температуры, реализуемые с помощью цилиндрического зонда Ленгмюра, и для исследования ионной концентрации и ионной температуры (в определенных границах) с помощью трехэлектродных сферических ионных ловушек.

Показаны характерные регистрограммы исследуемых параметров, полученных по телеметрическим каналам, обслуживающим советско-болгарский зондовый эксперимент. Вкратце рассмотрены некоторые особенности телеметрической записи в этом первом космическом эксперименте с участием Центральной лаборатории космических исследований Болгарской академии наук.

BULGARIAN ACADEMY OF SCIENCES

SPACE RESEARCH IN BULGARIA, 2

Sofia · 1979

First Results from Ionospheric Airglow Measurements Carried Out in Cuba

M. M. Gogoshev, S. K. Chapkunov, J. S. Gonzales, L. Palacio, G. Hill

Introduction

It is known that there is a large number of physico-chemical processes which bring the different atmospheric components into a state of excitation. A considerable part of the day airglow is emitted as a result of photoionizational excitation. For instance, the photoionization of the oxygen molecule can bring to excitation one or two oxygen atoms:

(1) $$O_2+h \text{ (from Sun)} \rightarrow O^*+O.$$

The atomic and molecular excitation of the upper atmosphere can also be provoked by collisions with the precipitating particles from the magnetosphere in a reaction of the following type:

(2) $$O+e \rightarrow O^*+e.$$

The electron in the left part of the expression (2) possesses energy slightly superior to the thermal energy of the electrons in the ionospheric plasma. The atomic or molecular excitation level depends on the electron or proton energy as well as on the cross-section of the interactions.

The ionospheric subthermal electrons, the so-called photoelectrons obtained during the photoionizational process, can also take part in reaction (2) during the day (*E*- and *F*-regions).

Particularly important is the contribution by the recombination aeronomical reactions, primarily by the so-called reactions of dissociative recombinations of the molecular ions in the irradiational ionospheric processes. The main reactions of that type are:

(3) $$O_2^+ + e \rightarrow O^* + O \qquad \alpha_D(O_2^+)$$

(4) $$NO^+ + e \rightarrow O^* + O \qquad \alpha_D(NO^+)$$

(5) $$N_2^+ + e \rightarrow N^* + N \qquad \alpha_D(N_2^+)$$

These reactions are of an order of 10^{-7} cm^3s^{-1} [1, 2] and their velocity constants are written at the right-hand side of the expressions.

Reactions (3), (4) and (5) operate diurnally and they play a particularly important role during the night, when there is no ionizing source. That is how the concentrations of electrons and of molecular ions are determined by these reactions. The quick disappearance of the molecular ions during the night is compensated on account of the ion-exchange reaction of the following type:

(6) $O^+ + O_2 \rightarrow O_2^+ + O$ velocity of K_2 according to [3].

In the ionosphere the aeronomical reactions of type (7) are around fifty in number or more. A review of these reactions in the ionosphere is offered in greater detail in [1-6] and in some other papers.

The examples given until now refer predominantly to the oxygen atoms and molecules, because they play the most important role in the *F*-region.

The irradiation of the atmospheric components can be obtained by the re-emission of some lines and bands of the solar light. This phenomenon takes pla ce mainly during the twilight but essentially it has no considerable effect on the airglow processes of the upper atmosphere.

It could safely be maintained that the airglow emissions from the aurora and from the upper atmospheric layers above the middle, low and equatorial latitudes are practically the same. The difference lies mainly in the intensity and in the fact that the polar emissions operate according to reaction (2), while at other latitudes reactions (1), (3), (4), (5) and (6) are valid. The theory of airglow emissions through the aurora and upper atmosphere can be found in [1].

Notwithstanding the fact that considerable progress has been made in the study of the upper atmosphere airglow and that there are many publications on this problem which show the connection between ionospheric processes and airglow, there is still no unanimous opinion on the nature of these connections. This is due mainly to the fact that until now the airglow emissions have been studied n an isolated manner. In such an eminent publication on atmospheric emissions s [1], these connections are treated mainly as being statistical in character, while one of the latest monographs published in 1975 on the ionosphere [7] contents itself with the description of the airglow-ionospheric connections obtained during the 1960's.

The purpose of this paper is to describe the first measurement results from the airglow emissions of the upper atmosphere carried out in Cuba and to show the connection existing between some of them and the ionospheric parameters measured there.

Selection of Measuring Emissions, Measuring Techniques and Equipment

In order to study the connections between the airglow emissions of the upper atmosphere and the ionospheric parameters, the best way is to choose emissions from the *E*- and *F*-layers. This is determined mainly by the presence of a relatively small number of atmospheric components and by the absence of complex molecular ions (e. g. negative ones). Furthermore, in order to reveal the physical connection of these parameters it is most convenient to choose the emission lines because, as it will be seen later on, they are best suited to photoelectric measurements.

The following emissions were selected for the purpose: First is the red oxygen line with λ 6300 Å of longitude (in fact this is the double 6300-6364). This line is emitted in the *F*-region. Second is the green oxygen line λ 5577 Å. It is

emitted mainly in the *E*-region (80-120 km), though about 15-20 per cent of its intensity is emitted in the *F*-region [8]. The third is one of the lines of the first negative system of the N_2^+ molecule. Its longitude is 4278 Å. The negative system is excited only by direct particle precipitation, and this provokes simultaneous ionization and excitation. Therefore, when controlling the emission, we can study the precipitation particle effects on the upper atmosphere.

In order to establish the quick variations of these emissions, which is particularly important for the phasic processes in the ionosphere, we have selected the two-filter photoelectric method. As we know, electrophotometry enables us to obtain a very high temporal resolution and, on the other hand, the sensitivity of this technique greatly exceeds that of the photographic method.

The two-filter technique has been chosen for the following considerations: The latitude of each one of the selected emissions is of the order of 10^{-2} Å (at normal ionospheric temperatures). There exists no filter with such resolution. The filters used in the equipment have a half-latitude of 50 Å. Therefore, each filter together with the emission is also pervious by the spectral phone. We used

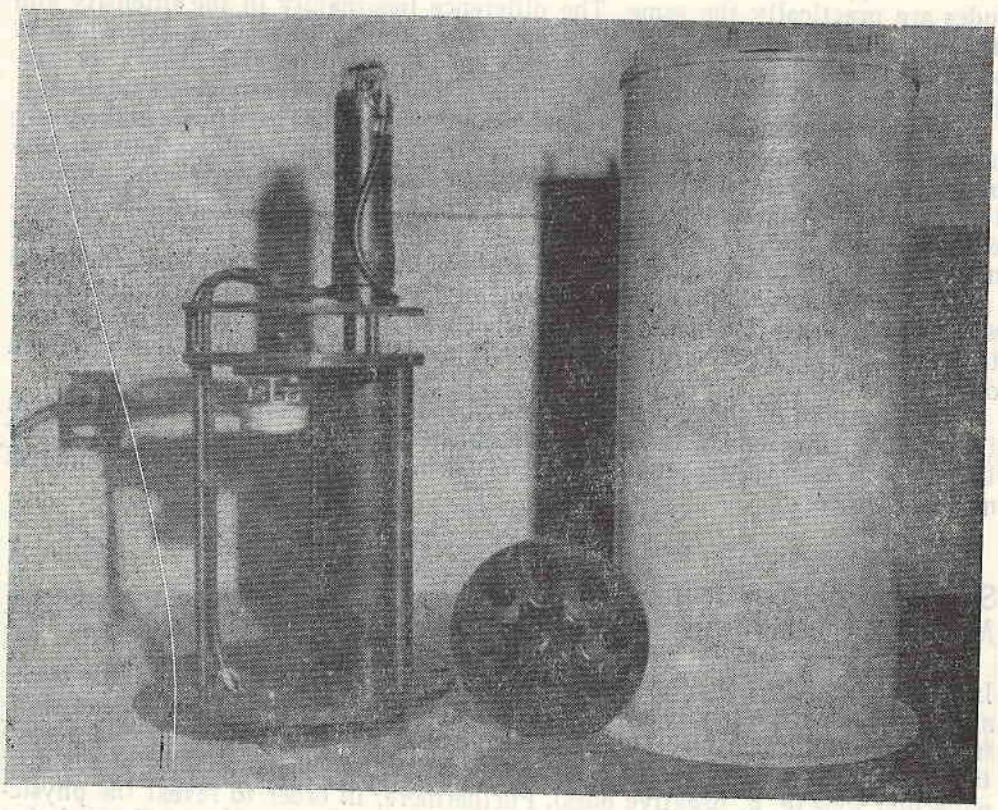

Fig. 1

a second filter in order to isolate the phone, and by that filter we measured the phone close to the emission.

The electrophotometer used for the observations consisted of an optical system (full angle — 10°), a disk with interference filters, and a photoreceiver —

photomultiplier FEU-79. The principle blocks are shown on Fig. 1. Besides the six photofilters, there were two more positions on the disk — one for the measurements of the dark current and another one for mounting the photostandard for the purpose of continuous control over the sensitivity of the equipment. The disk with the photofilters was rotated by a motor provided with reduction gear. More detailed information about the equipment used can be found in [9], and

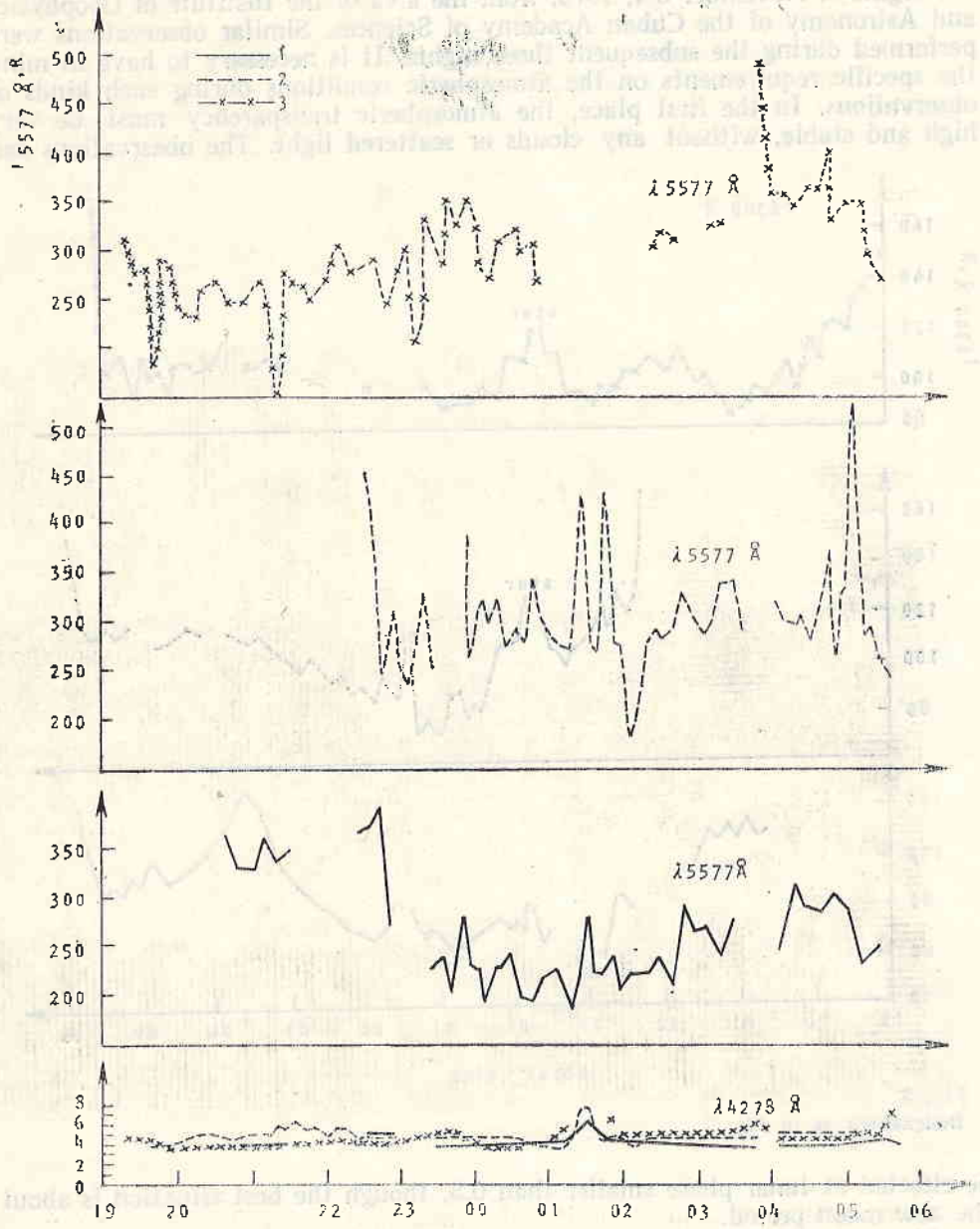

Fig. 2
1 — November 3-4, 1975; *2* — November 4-5, 1975; *3* — November 5-6, 1975, (Havana)

greater details on the electron blocks are to be found in [10]. The technique of information processing is described in [4].

Measurement Results

In Cuba, the first observations on atmospheric emissions were carried out during the nights of November 3-4, 1975, from the area of the Institute of Geophysics and Astronomy of the Cuban Academy of Sciences. Similar observations were performed during the subsequent three nights. It is necessary to have in mind the specific requirements on the atmospheric conditions during such kinds of observations. In the first place, the atmospheric transparency must be very high and stable, without any clouds or scattered light. The obesrvations can

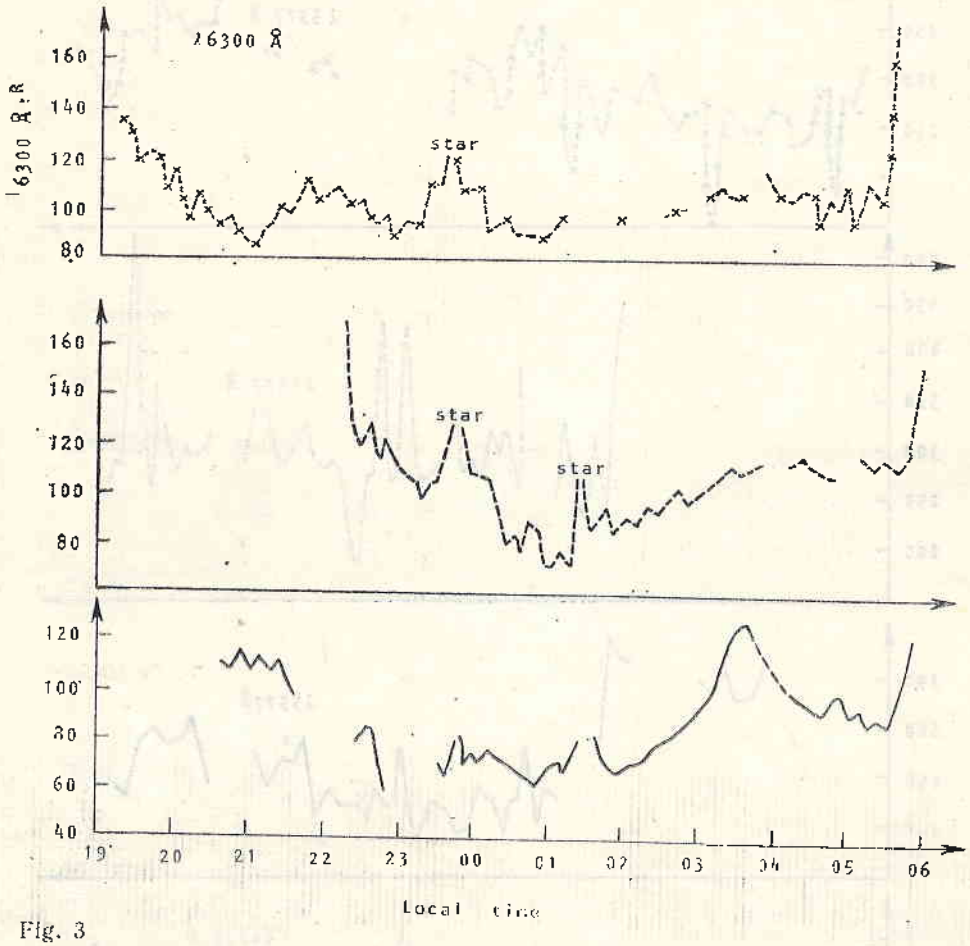

Fig. 3
Designations as in Fig. 2

be effected at lunar phase smaller than 0.5, though the best situation is about the new moon period.

The behaviour of the intensity of the measured atmospheric emissions, depending on the time, is shown in Fig. 2 (green and blue lines) and in Fig. 3 (red

line). The threshold sensitivity of the equipment for all three lines is of the order of 4-5 R. The relative error of the measurements is 5 per cent and the temporal resolution is 6-7 min (i. e. two neighbouring values are divided by an interval of 6-7 min for one emission).

The behaviour of the green emission which had been observed for four nights did not differ distinctly from the measurements of this line at midlatitudes — cf. [1, 4, 8, 11]. The emission intensity changed within the range of 190-400 R, which was the normal limit for disturbed conditions. Quick intensity fluctuations were typical here, as in the case of the midlatitudes. This was explained by the fact that the red emission was irradiated in the *E*-region in the range of 80-120 km at a reaction of the following type:

$$O+O+O \rightarrow O_2+O(^1D). \tag{7}$$

This reaction, initially suggested by Chapman, is known as the triple collision. Therefore, oxygen concentration fluctuations (atmospheric density) can strongly influence the intensity of the emission. It is also well known that strong atmospheric turbulence takes place in the region of 100-120 km.

It was interesting to follow the behaviour of the 4270 Å emission during the nights already mentioned (Fig. 2). It can be seen that the intensity of this line changed within a narrow range of 3-4 R. As we have already observed (Section 2), the threshold sensitivity of the equipment was of the order of 4-5 R, and the measurement error was about 5 per cent. Therefore, we can assume with certainty that there was no emission of the 4278 Å line during these nights, i. e. no particle precipitation had taken place. The increase of the order of 7 R recorded at 01:30 was probably due to the pass of a star source through the angle field of the apparatus.

The behaviour of the red line will be examined further on.

Correlation between the Irradiation of the Red Oxygen Emission and Some Parameters of the F-Region

It has been shown by D. Barbier [12] that between $f.F$ and and $h'F$ parameters of the night F-region and the irradiation of the red oxygen line there exists a definite relation of the following type:

$$I_{6\,300}=K(f_0F)^3 \exp\left(-\frac{h'F-200}{H}\right)+C, \tag{8}$$

where f_0F is the critical frequency and $h'F$ is the operative height of the F-region, while H is the scale height. K and C are two constants determined for each station separately during simultaneous ionospheric and optical observations.

On the basis of a more up-to-date theory of the region, Serafimov and Goshev worked out a new formula in 1972 which is similar to (8), with the empirical constant K of formula (8) now being the following:

$$K=1.24\times10^4 \cdot R_2[O_2]_{200}, \tag{9}$$

where $K_2=4.10^{-11}$ cm^{3}s^{-1} [3, 6] is the rate constant of exchange reaction (6) and $[O_2]_{200}$ is the molecular oxygen density at 200 km level.

Other publications (e. g. [13, 14]) show the use of the N_e (h) profile for the calculation of the red emission theoretical profile.

Figure 4 shows the behaviour of the λ 6300 Å line intensity (by observations) for the night of November 3-4, 1975, and also the behaviour of f_0F and $h'F$ by observations at the San Jose ionospheric station. Since November 3rd was a magnetically quiet day as regards the solar activity (see Table 1), coefficients K and C

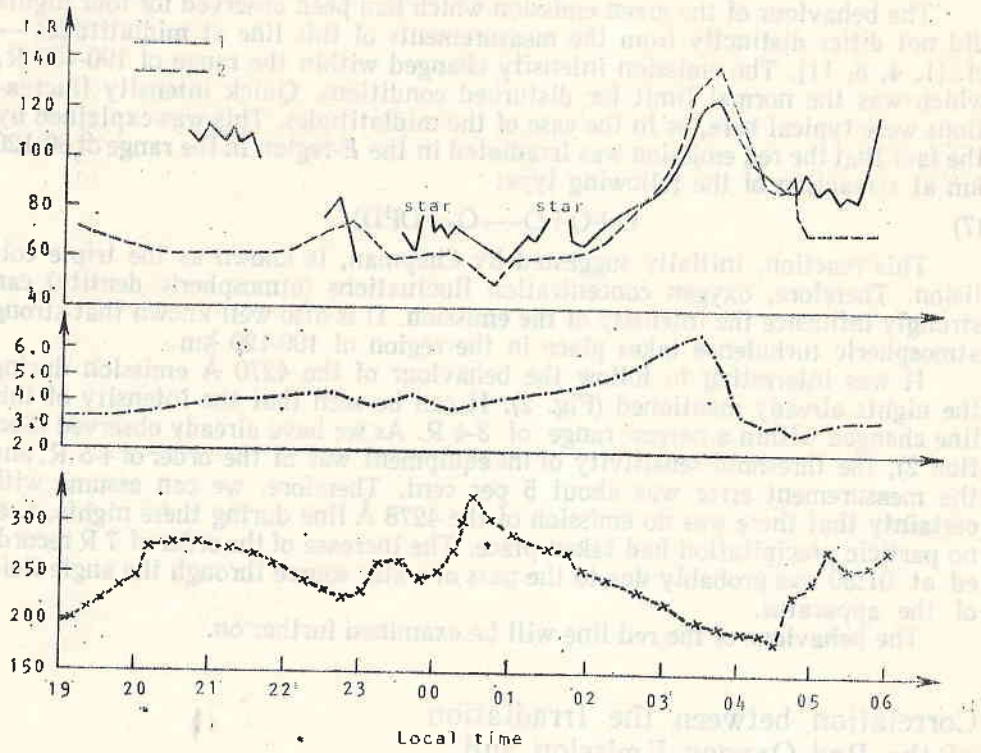

Fig. 4
1 — I_{6300} experimental (November 3-4, 1975, Hawaii); *2* — I_{6300} theoretical

were calculated, having the following values: $K=1.96$ and $C=60$ R by the correlation function

$$I_{6300}=f\left[(f_0F)^2 \exp\left(-\frac{h'F-200}{H}\right)\right]. \tag{10}$$

After that, using formula (8), the theorerical intensities of the red emission were calculated as shown on Fig. 4.

It should be borne in mind that, on account of the clouds, the apparatus had to be switched off several times (see interval 21:30-22:30; 22:30-22:45; 22:45-23:30). Theoretical-to-experimental data scatter appears during the night and immediately before the morning hours. There was good agreement between theory and practice during the 23:00-04:30 interval. In fact, as shown in [15], formula (8) and the other similar formulas give the rate of the ionospheric recombination. Therefore, Fig. 4 can be interpreted in the following manner: the red emission increase which begins at about 01:00 is due only to the dissociative recombination increase given by formula (3). But it is still difficult to suggest the reasons for that increase.

Before examining the emission behaviour during the other days, we shall examine the solar and geomagnetic activity levels for one period of observa-

tion. Data from solar observations were obtained at the Observatory of the Institute of Geophysics and Astronomy of the Cuban Academy of Sciences, with the exception of the radioemission in the range of 10 cm — Boulder. They are given in Table 1.

Table 1

November	1	2	3	4	5	6	7	8	9	10
Radioemission 2 cm	515	516	517	519	523	525	525	526	524	522
Radioemission 4 cm	149	150	151	154	157	159	159	159	156	155
Radioemission 10 cm	72	73	74	77	80	82	82	83	80	80

The radioemission data are given in 10^{-22} w/m^2 Hz units.

According to the data obtained, the first days of November were quieter. Over a period of three days — from the 1st to the 3rd November, the radioemission increased from 72 to 74 units. On the 4th day it had already risen to 77, and on the 5th day it rose to 80, remaining constant on the 6th and 7th days. The inten-

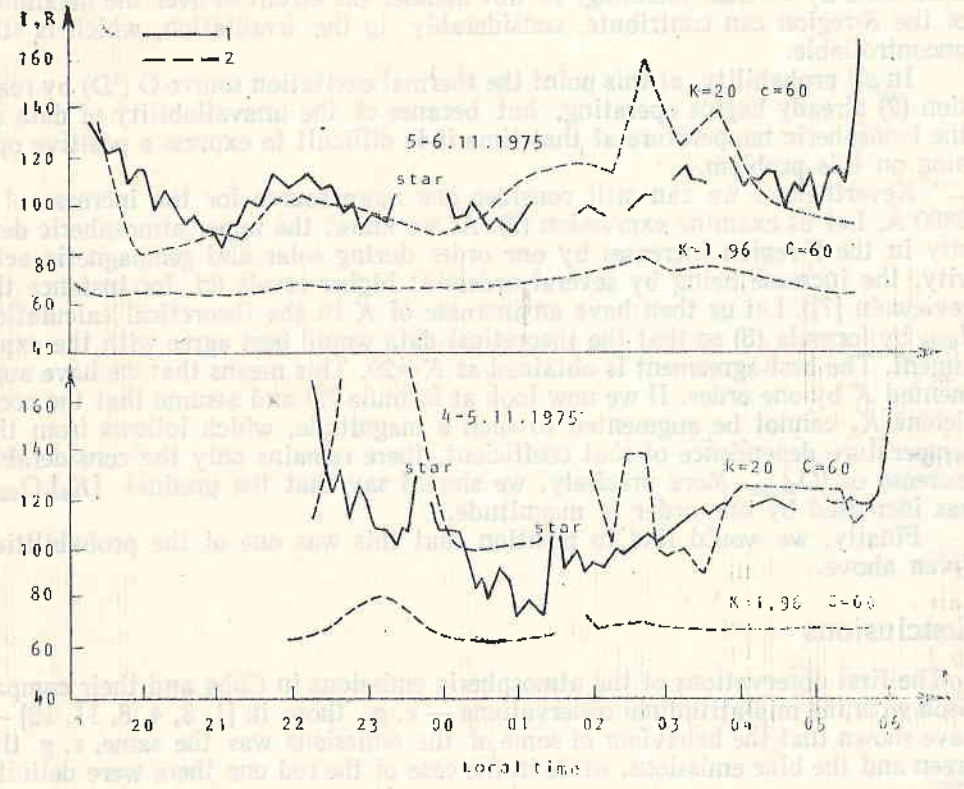

Fig. 5
1 — experimental; 2 — theoretical

sity decreased after the 8th day. The magnetic data show that a magnetic disturbance had set in on the second day and that its maximum appeared about the 4th to the 5th November.

Resulting from the increase in solar and geomagnetic activity, there appeared a gradual intensity increase of the red emission, as can be seen in Figs. 4 and 5. Thus the minimum night intensity on the 3rd and 4th November was already of the order of 60 R. On November 4-5 it became of the order of 80 R, and on November 5-6 it rose to more than 90 R.

A bright star source crossed the zenith about 23:45 and 01:30 of the first night, and this resulted in an intensity increase. The disturbance of the peak during the other nights 4-5 minutes earlier than during the first night confirms the fact that it was really a star source.

In addition to the intensity increase, which was probably due to the solar activity increase, we examined yet another important detail. This was the scatter between the experimental and the theoretical data for November 4-5 and 5-6, when in calculating them we used the same constants as for the November 3-4, namely, $K=1.96$ and $C=60$ R. This phenomenon probably has a bearing on the negative ionospheric disturbance during that time — probably the result of the geomagnetic storm. This was immediately to be observed in the night drop of the critical frequencies.

As it is known, one of the suggestions made for explaining such a drop is the redistribution of the electron density in height, which cannot possibly be controlled by vertical sounding. In this manner the electrons over the maximum of the F-region can contribute considerably to the irradiation, which is still uncontrollable.

In all probability, at this point the thermal excitation source O (^{1}D) by reaction (2) already begins operating, but because of the unavailability of data on the ionospheric temperature at that time it is difficult to express a positive opinion on this problem.

Nevertheless, we can still consider one more source for the increase of λ 6300 Å. Let us examine expression (9). As we know, the upper atmospheric density in the F-region increases by one order during solar and geomagnetic activity, the increase being by several orders at higher levels (cf. for instance the review in [7]). Let us then have an increase of K in the theoretical calculation I_{6300} by formula (8) so that the theoretical data would best agree with the experiment. The best agreement is obtained at $K=20$. This means that we have augmented K by one order. If we now look at formula (9) and assume that the coefficient K_2 cannot be augmented to such a magnitude, which follows from the temperature dependence of that coefficient, there remains only the considerable increase of $[O_2]_{200}$. More precisely, we should say that the product $[K_2].O_{2200}$ has increased by one order of magnitude.

Finally, we would like to mention that this was one of the probabilities given above.

Conclusions

1. The first observations of the atmospheric emissions in Cuba and their comparison with the midlatitudinal observations — e. g. those in [1, 3, 4, 8, 11, 12] — have shown that the behaviour of some of the emissions was the same, e. g. the green and the blue emissions, while in the case of the red one there were definite differences.

2. In Cuba, the red emission, which represents the rate of the night recombination process, shows a definite increase after midnight. This results from the dissociative recombinational increase in the F-region. These processes are probably related to the increase of the critical frequencies f_0F after midnight, as described in [17], but their physical mechanism is still unclarified.

3. The first night observations of the 4278 Å emission, though only for three nights during a disturbed period (the maximum K index at that time was $K=4$), showed no remarkable particle precipitation. In any case, if we use the technique given in [18, 19] and keep into consideration the fact that the intensity of λ 4278 Å was close to zero, we are entitled to maintain that the upper boundary of the precipitated electron flux, i such does exist, is below 2×10^{-2} erg/cm^2 s.

The authors express their gratitude to Professor Kiril Serafimov, Director of the Central Laboratory for Space Research in Sofia, and to Dr. Rosando Alvarez, Director of the Institute of Geophysics and Astronomy in Havana, for the all-round help rendered by them during the organization of these observations in Cuba.

References

1. Чемберлейн, Г. Физика полярных сияний и излучения атмосферы. Москва, 1963.
2. Серафимов, К. Физика средней ионосферы. София, БАН, 1970.
3. Serafimov, K., M. Gogoshev. Report to the Nat. Scientific Session for Astronomy and Astronaut., Oct. 17-23, 1971, Stara Zagora, 1972.
4. Гогошев, М. Кандидатска дисертация, БАН, София, 1973.
5. Swartz, W. E. — Ionosph. Res. Sci. Rep., 381, Penn. St. Univ., 1972.
6. Fehsenfeld, F. C., F. D. Goldan, A. L. Schmeltekopf, E. E. Ferguson. — Plan. Space Sci., **13**, 1965, 579.
7. Ришбет Г., О. К. Харпот. Введение в физике ионосферы. Ленинград, 1975.
8. Gogoshev, M. PAGEOPH, vol. III, 1973/x, 2300, Basel.
9. Gogoshev, M., S. Chapkunov. — Space Res. in Bulgaria, **1**, 1978, 73.
10. Chapkunov, S., M. Petrounova. — Compt. rend. Acad. bulg. sci., **29**, 3, 1976, 347-349.
11. Д. Бейтс. Сб. физ. верхней атмосферы, под редакцией Г. Радклиффа, Москва, 1963.
12. Barbier. D. — Géophysique Extérieure. New York-London, 1963.
13. Wickwar, V. B., L. L. Coger, H. C. Carlson. — Planet. Space Sci., **22**, 1974, 709.
14. Serafimov, K., M. Gogoshev. — Preprints COSPAR, Varna, Bulgaria, 1975.
15. Serafimov, K., M. Gogoshev. — Compt. rend. Acad. bulg. sci., **25**, 2, 1972.
16. Gogoshev, M., K. Serafimov. — Compt. rend. Acad. bulg. sci., **25**, 2, 1972.
17. Lazo, B., L. Palacio. — Communicationes No. 15, 1974.
18. Dalgarno, A. — Ann. Geophys., **20**, 1964, 1.
19. Гогошев, М. О высипании частиц в верхней атмосфере средних широт. — Доклады БАН, 1972.

Первые результаты измерения оптических эмиссий ионосферы, проведенного на Кубе

М. М. Гогошев, С. К. Чапкынов, Х. С. Гонзалес, Л. Паласио, Ж. Хил

(Резюме)

В введении рассмотрены физические основы существования оптических эмиссий ионосферы. Внимание уделено фотоионизирующим процессам в дневных условиях. Рассмотрены процессы диссоциативной рекомбинации молекулярных ионов в ионосфере.

Целью работы является описание первых результатов измерения оптических эмиссий ионосферы, полученных с помощью болгарской электрофотометрической аппаратуры на территории Республики Куба.

Описана измерительная техника и применяемые при измерениях технические средства; обращено внимание на выбор измеряемых эмиссий.

Приведены результаты измерений и сделаны выводы на основе первых измерений естественных атмосферных оптических эмиссий, проведенных болгаро-кубинским коллективом на Кубе. Дано сопоставление с аналогичными экспериментами, проведенными в средних широтах, и указаны некоторые особенности измерения в низких широтах.

BULGARIAN ACADEMY OF SCIENCES

SPACE RESEARCH IN BULGARIA, 2

Sofia · 1979

The Negative Ions in the *F*-Region under Night Conditions

K. B. Serafimov

It was believed until recently that the negative ions limit their effects at night to the height of the night *E*-layer (about 120 km — cf. [1, 2, 3]). However, a number of new studies have indicated that notwithstanding the low densities of the negative ions, their integral abundance is significant and, taking into account their activity in a number of basic aeronomical processes, it will become necessary to undertake a basic re-examination of their role [4, 5, 6]. For instance, it is stated in [6] that at high geomagnetic latitudes the abundance of negative ions in the *F*-region is sufficient for them to contribute essentially to the neutralization processes, i. e. the ion-ion recombination in the circumpolar regions between the positive and the negative ions in the high ionosphere is not negligible. On that basis it would be necessary to re-examine the neutralization processes and to assess the role of the dissociative recombination in the above geographic regions. In addition to that, as a sequence of the essential influence of the ion-ion recombination, we should find a considerable portion of oxygen atoms in a $O(^1D)$ state, which are emitted by the red oxygen line λ_w 6300 Å in the spectrum of the night airglow. However, this line is generated also at the dominant neutralization mechanism — the dissociative recombination which also leads to considerable $O(^1D)$ densities. It has been pointed out in [4, 5] that the negative ion densities in the *F*-region are so low that their role in the neutralization processes and in the generation of the red line is negligible. The aim of our present work was to create a model for the altitudinal and seasonal variations of the coefficient of the negative ions λ in the *F*-region, through which to provide objectification for the examination of that problem, both for the aims of the studies of the neutralization processes and of night airglow and for the independent morphological investigation of the ionosphere, the analysis of the night plasmasphere included.

Initial data for the development of models for the variations of the negative ion night coefficient in the high and outer ionosphere in the work undertaken will be provided by the international models for the neutral atmosphere — CIRA 72 (see [7] and for the ionosphere [8]). The CIRA-72 model has many deficiencies, particularly under low solar activity, but we shall not dwell on them here. Similar is the situation with the International Model for the Ionosphere [8], which is still far from being a unified representation of the average

night conditions. In particular, we showed a group of Bulgarian ionospheric models in [9] which, at medium geographic latitudes at least, offer better approximations to the real ionosphere. Particularly convenient for the above-maximal, outer ionosphere, in which the negative ions have their influence, is the model developed in [10] which provides for convenient analytical calculations. Notwithstanding the deficiencies of the international models, at the present stage they are the only internationally accepted approximation to reality, and on that account they are at the basis of the present work.

The generation of the negative ions takes place mainly through the radiative attachment reaction, and these ions are almost entirely of the atomic oxygen on account of its familiar electron affinity

$$O + e \longrightarrow O^- + h\nu, \quad K_1 \tag{1}$$

where $h\nu$ is a continuum photon ($\lambda_w < 8463$ Å), as the coefficient K_1 of (1) is in accordance with [11]: $K_1 = 1.3 \times 10^{-15}$ cm^{3}s^{-1}. Part of the negative ions disappear by an associative detachment reaction

$$O^- + O = O_2 + e^-, \quad K_2 \tag{2}$$

where the velocity $K_2 = 1.4 \times 10^{-10}$ cm^{3}s^{-1} [12], while the other essential part is involved in the ion-ion recombination:

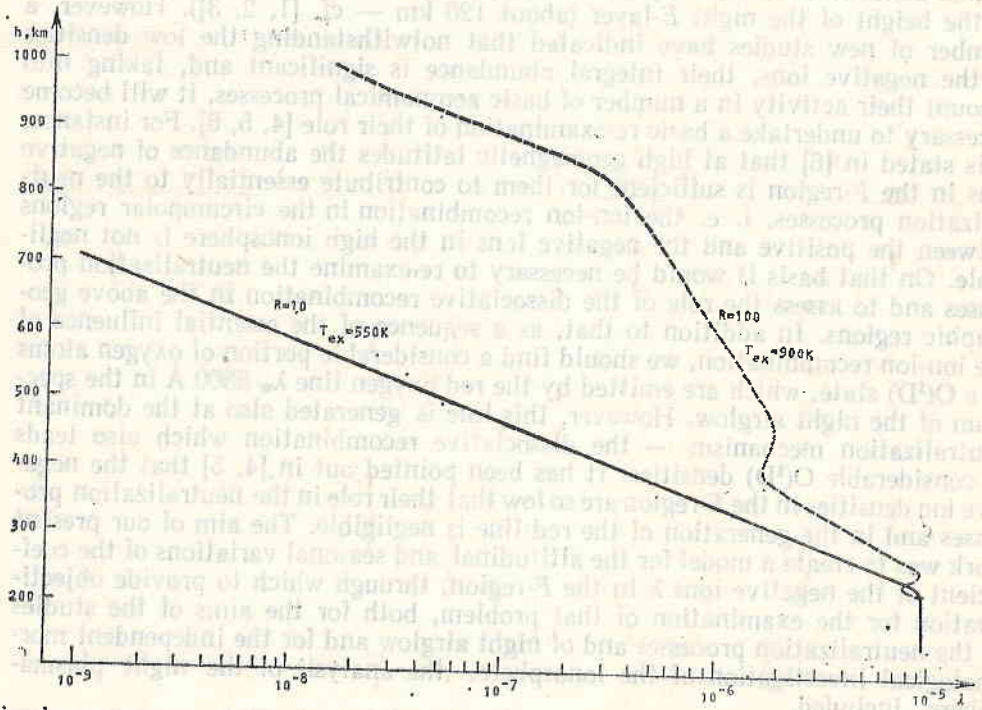

Fig. 1

$$O^+ + O^- \longrightarrow O^* + O^* + KE, \quad K_3 \tag{3}$$

where the velocity $K_3 = 1.5 \times 10^{-7}$ cm^{3}s^{-1} [5, 13].

Consequently, the equilibrium equation of the negative oxygen ions in the *F*-region for the photochemical processes in first approximation will be

(4) $$\frac{d[O^-]}{dt} = K_1[O]N_e - \{K_2[O] + K_3[O^+]\}[O^-].$$

Under conditions of equilibrium we have

(5) $$O^- = \frac{K_1[O]N_e}{K_2[O] + K_3[O^+]} = \frac{K_1[O]N_e}{K_2O + K_3R_eN_e},$$

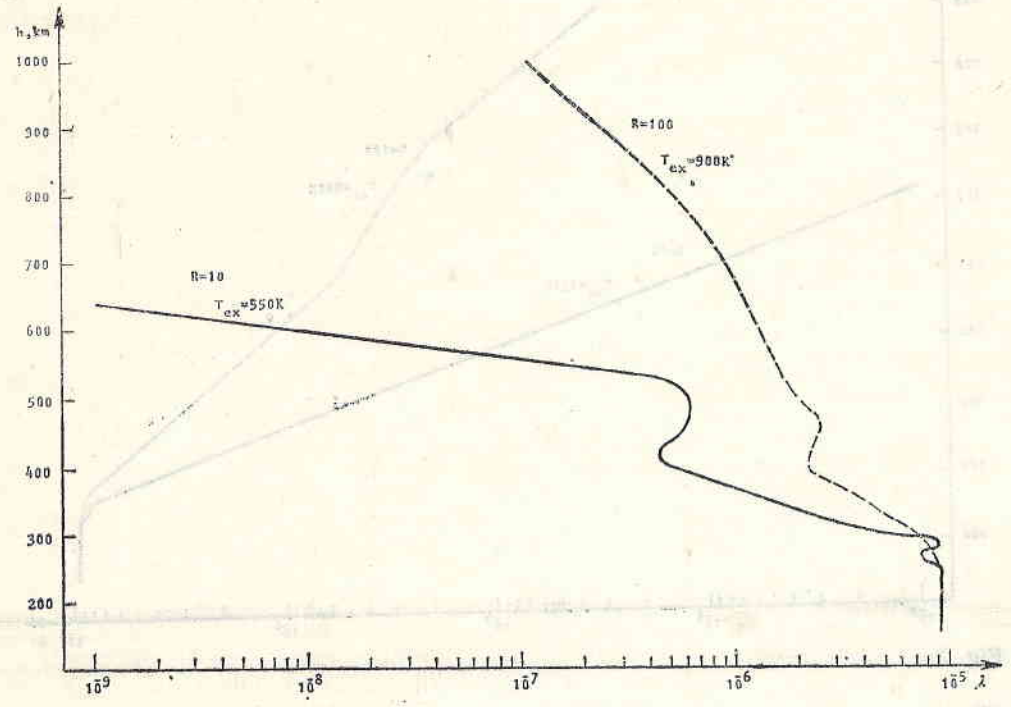

Fig. 2

where $R_2(h)=[O^+]/N_e$, and N_e is the electron density which, just as [O], $[O^+]$ and R_e, is a function of the altitude h.

The models for the $[O^-]$ distribution can be obtained from (5) by using the profiles for $[O_2]$ (h) for the CIRA-72 model under different conditions and the model for O^+ (h) from [8]. For the sake of convenience we here propose models for the coefficient of the negative ions λ determined by

(6) $$\lambda = \frac{[O^-]}{N_e} = \frac{K_1[O]}{K_2[O] + K_3[O^+]}.$$

From [7, 8] we can obtain averaged approximating models for the variations of λ which may be applied to concrete profiles $N_e(h)$ obtained, in order to calculate the density $[O^-]$ by means of (6). Of course, this will be a first approximation which makes it possible, under any normal conditions, using a profile $N_e(h)$ obtained from vertical probing (with ionospheric stations or rockets), from the incoherent scatter, or by any other method, to determine the profile of the negative ions $[O^-](h)$by using a model for the standard averaged values of λ. Likewise, using such a model of λ, it is possible to restore any value for $[O^-]$ at a given altitude, geographic conditions and phase of solar activity.

The data on N_e and $[O^+]$ in [8] are provided for two levels of solar activity — at $R=10$ and at $R=100$, where R is the average monthly number of the sunspots. The transition from these data about the solar activity to the parameter used in [7], namely, the exospheric temperature (T_{ex})is done as in [14], according to the following dependence

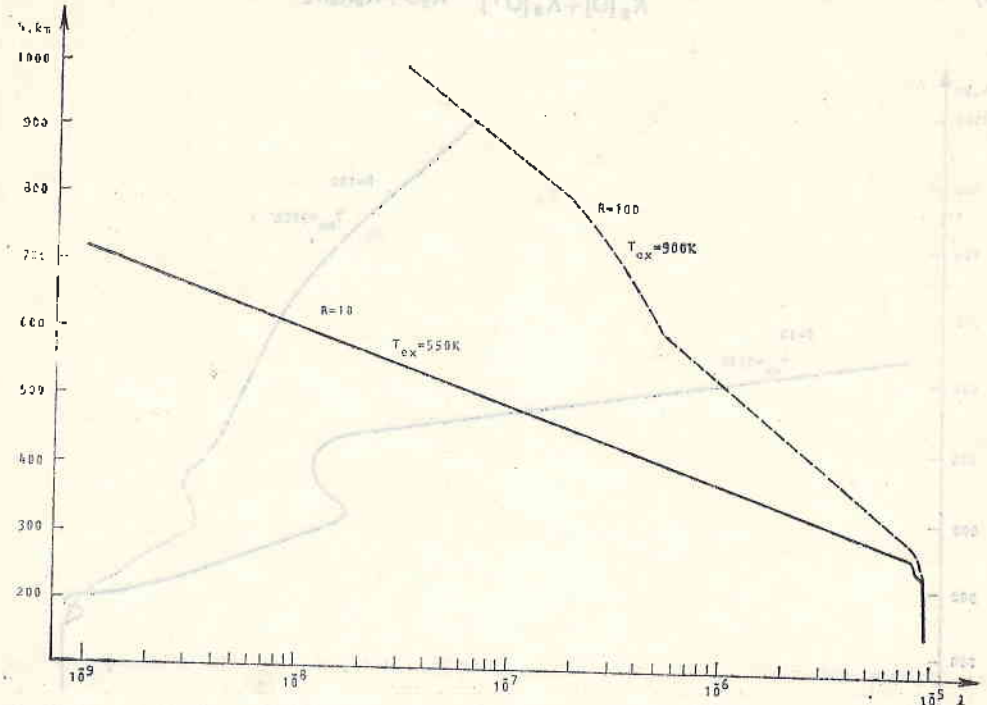

Fig. 3.

(7) $$\overline{T}_{ex}\approx 513+3.4\,\overline{R}.$$

Hence at $\overline{R}=10$ we have $\overline{T}_{ex}=550$ K, while at $\overline{R}=100$ the corresponding $T_{ex}\approx 900$ (in first approximation, according to the available data on T_{ex} in [7]).

The models obtained for the variations of λ according to initial data of the international models [7, 8] for 00:00 h local time have been shown in Fig. 1 — for the 6th month at $\varphi=45^0$ and for both levels of solar activity, in Fig. 2—for the 9th month and $\varphi=45^0$, in Fig. 3 — for the 12th month and $\varphi=45^0$, and in Figs. 4 and 5 — for the months of June and January, respectively, though at $\varphi=18^0$.

From Figs. 1, 2, 3, 4, 5 it is possible to deduce the following principal laws related to the altitudinal, latitudinal, cyclic and seasonal specifics of the coefficient of the negative ions λ:

1. The maximum value of λ is at the beginning of the F-region where, under any conditions up to altitudes of 220 km we gave

(8) $$K_2[O]\gg K_3[O^+].$$

It follows in this case that

(9) $$\lambda=\frac{K_1}{K_2}=0.93\times 10^{-5}.$$

2. The absolute values of λ in the F-region are rather low and they always remain below the value of 0.93×10^{-6}.

3. At low solar activity for the sector $h\geqslant h_{m}F$ the distribution of $\lambda(h)$ is close to the exponential one, with the exception of the equinoxes. With the rise in the solar activity there occurs a considerable complication in the $\lambda(h)$ profile,

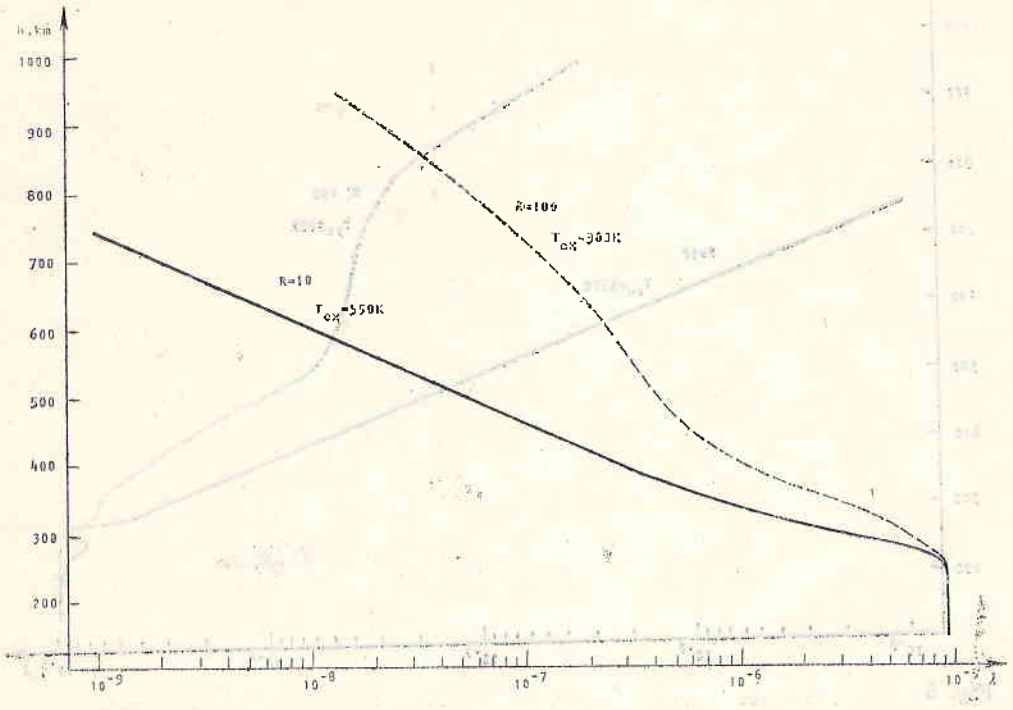

Fig. 4

showing a number of extrema and inflex regions in the summer and at the equinox periods.

4. The rise in the solar activity is accompanied by a sharp rise in the values of λ, the rise reaching one order and more for the above-maximal outer ionosphere. Since the model value of R for high activity used by us, $R=100$, is far from being maximal, it follows that λ may have higher values as well, though always lower than the limiting value (9).

5. At mid-latitudes the seasonal run shows maxima of λ for most of the F-region during equinox and two slightly outlined maxima during the summer and winter.

6. The $\lambda(h)$ profiles for relatively low geographic latitudes ($\varphi=18°$) are generally of the same nature as at mid-latitudes and bear confirmation for the regularities 1, 2, 3 and 4 mentioned above.

7. Under low solar activity λ shows no particular geographic variations in the latitudinal interval of 18 to 45°. At high activity the increase in the geographic latitude within the above interval is accompanied by a rise in λ as well.

The absolute values of the night densities of the negative ions $[O^-]$ are of particular interest. By way of example, Fig. 6 shows the respective altitudinal profiles $[O^-](h)$ for 00:00 h of the month of June at $\varphi=45°$ for both levels ($R=$

$=10$ and $R=100$) of the solar activity according to the data for λ in Fig. 1 and the electron density model [8]. It is obvious that there is a considerable increase in the ion density $[O^-]$ at high solar activity. The total number of the negative ions in the F-region

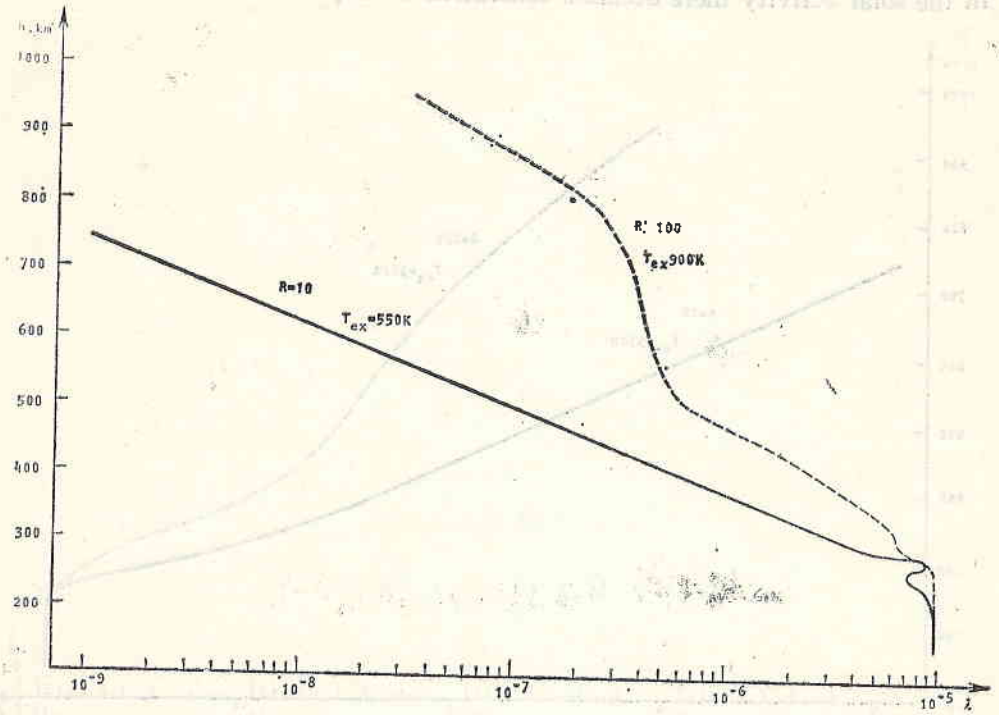

Fig. 5

$$N_g^- = \int_{160}^{1000} [O^-]\,dh \tag{10}$$

is obtained in the order of 10^7 ions per column of 1 cm^2 cross-section (in the example examined from Fig. 6, this number at $R=100$ is approximately 3.35×10^7 cm^{-2}). According to the data in [1, 2, 3], the averaged abundance of negative ions in the vertical column of the night D-region is about 10^8 up to several times 10^9 cm^{-2}, the total amount of O^- ions in the vertical column varying from 10^6 to 10^8 cm^{-2}. It is obvious that the total abundance of O^- negative ions in the D-region and in the F-region is comparable during the night, notwithstanding the very low densities of these ions in the high ionosphere. Of course, the integral number of the negative ions in the night D-region is appreciably larger than in the night F-region, mainly at the expense of ions heavier than the O^- ion.

It should be pointed out that there are only assumptions about the densities of the negative ions in the night F-region in the equatorial and circumpolar regions. It has been assumed in [6], for instance, that the role of the ion-ion recombination and of the negative ions increases poleward, because there is a density increase of atomic oxygen compared to molecular oxygen. It is obvious that this will raise λ and O^-, but at the rather frequent excessive increases of the elec-

tron density at high geographic latitudes λ will decrease to its value at average conditions.

The low ion densities of O^- may lead to certain interesting effects, particularly in the case of local measurements. For instance, if we compare the local

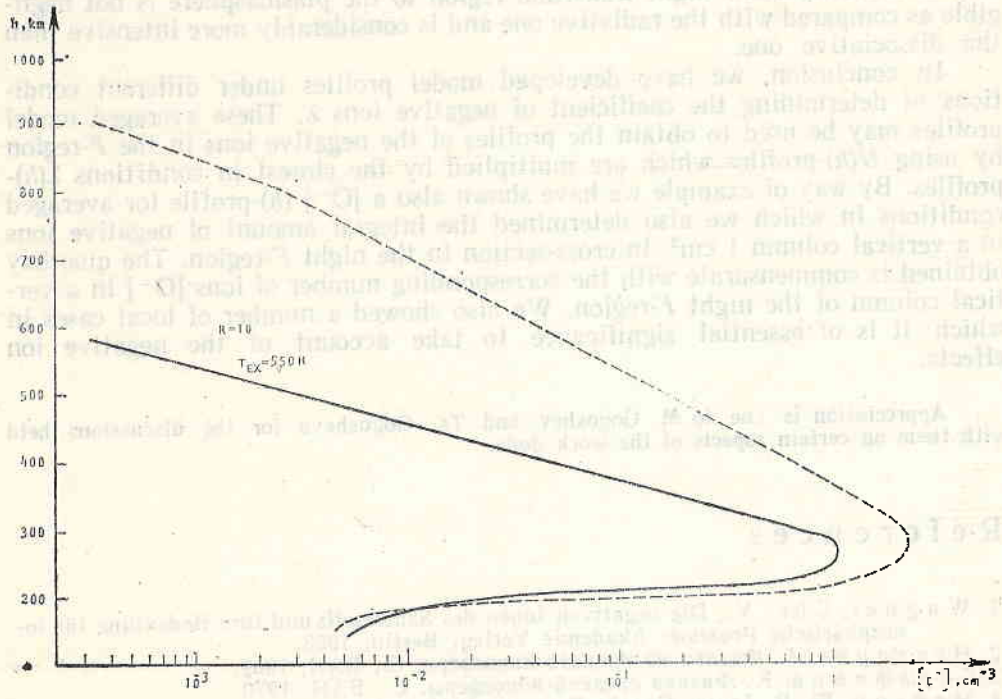

gFi. 6

intensity of the night airglow obtained from the dissociative I^d_{6300} and from the ion-ion recombination I^i_{6300} we shall obtain the following expression:

$$\frac{I^i_{6300}}{I^d_{6300}}=\frac{A}{A_{6300}}\cdot\frac{\beta_{6300}K_1K_2[O][O^+][1+B(h)]}{A_{6300}\{K_3[O^+]+K_2[O]\gamma_1[O_2]\}}, \tag{11}$$

where $B(h)=\frac{\gamma_1[O_2]}{\alpha_1 N_e}+\frac{\gamma_2[N_2]}{\alpha_2 N_e}$, the coefficients γ_1 and γ_2 are the rates of recharging the oxygen and nitrogen molecules respectively with the oxygen atomic ions, while d_1 and α_2 are the coefficients of dissociative recombination of O_2^+ and NO^+; $A=0.0091\ s^{-1}$; $A_{6300}=0.0069\ s^{-1}$; $\beta=0.12$.

Under different conditions the ratio (11) becomes equal to or bigger than unity for h equal to 500-600 km. Under the average conditions of the examined models for a height of 600 km the ratio (11) is 6, and this signifies that at these altitudes there is a decisive predominance of the ion recombination over the dissociative one, and the local airglow is defined from the ion-ion recombination. However, the local intensity of this airglow is much lower than that at altitudes of 200 to 300 km where the predominant generating mechanism of the red oxygen line is the dissociative recombination. That is why, the examination of the ion-

-ion recombination only at high altitudes ($h > 500$ km), is justified taking into account the local problems.

It is of essential significance that at very high solar activity the recombination of O^+ at altitudes of about 600 km is determined practically by the commensurate action of the ion and radiative recombination. The ion-ion recombination in this important night transition region to the plasmasphere is not negligible as compared with the radiative one and is considerably more intensive than the dissociative one.

In conclusion, we have developed model profiles under different conditions of determining the coefficient of negative ions λ. These averaged model profiles may be used to obtain the profiles of the negative ions in the F-region by using $N(h)$-profiles which are multiplied by the closest in conditions $\lambda(h)$-profiles. By way of example we have shown also a $[O^-]$ (h)-profile for averaged conditions in which we also determined the integral amount of negative ions in a vertical column 1 cm^2 in cross-section in the night F-region. The quantity obtained is commensurate with the corresponding number of ions $[O^-]$ in a vertical column of the night F-region. We also showed a number of local cases in which it is of essential significance to take account of the negative ion effects.

Appreciation is due to M. Gogoshev and Ts. Gogosheva for the discussions held with them on certain aspects of the work done.

References

1. Wagner, Chr. V. Die negativen Ionen des Sauerstoffs und ihre Bedeutung für ionosphärische Prozesse. Akademie Verlag, Berlin, 1963.
2. Несторов, Г. Физика на ниската йоносфера. С., БАН, 1969.
3. Серафимов, К. Физика средней ионосферы, С., БАН, 1970.
4. Hanson, W. B. Journ, Geoph. Res., 75, 1970, 4343.
5. Van Zandt, T. E., B. A. Tinsley. — Ann. Geoph., 30, fasc. 1, 1974, 21.
6. Tinsley, B. A., J. A. Bittencourt. — Journ. Geoph. Res., 80, 16, 1975, 2333.
7. COSPAR Int. Ref. of Atm. — CIRA 1972, Akademie Verlag, 1973.
8. Rawer, K., S. Ramakrishnan, D. Bilitza. Preliminary Reference Profiles for Electron and Ion Densities and Temp. prop. for the Int. Ref. Ionosphere, I, PW-Sci. Rep. W. B. 2, 1975.
9. Серафимов, К. — Съобщения, VII, № 3, 1977.
10. Serafimov, K. — Compt. Rend. Acad. Bulg. Sci., 30, 1977.
11. Massey, H. S. W. Electronic and ionic impact phenomena. 2, London, Oxford and the Clarendon Press, 1969, 1265.
12. Fehnsenfeld, F. C., A. L. Schmeltekopf, D. B. Dunkin, E. E. Ferguson. — ESSA Tech. Rep. ERL 135—AL-, Sept. 1969.
13. Olsen, R. E., J. R. Petersn, J. Moseley. — Journ. Geoph. Res., 76, 1971, 2516.
14. Серафимов, К., М. Гогошев, Ц. Гогошева. — Геомагнетизм и Аэрономия, XVII, 1977.

Отрицательные ионы в ночной F-области

К. Б. Серафимов

(Резюме)

Используя международные модели нейтральной атмосферы и ионосферы, в работе решены уравнения баланса для отрицательных ионов в F-области. Получен коэффициент отрицательных ионов λ, максимальное значение которого не превышает 1.10^{-5}. Сделаны выводы об ожидаемых сезонных и пространственных вариациях λ.

Дана оценка интегральной плотности отрицательных ионов на высоте свыше 160 км порядка 10^7 см$^{-2}$. Дано сравнение локальной интенсивности свечения ночного неба, являющегося результатом диссоциативной и ионно-ионной рекомбинации. Вклад обоих механизмов соизмерим на высотах 500—600 км.

BULGARIAN ACADEMY OF SCIENCES

SPACE RESEARCH IN BULGARIA, 2

Sofia · 1979

Analysis of the Results of Mass-Spectrometric and Probe Measurements Carried Out on Intercosmos-12

G. L. Gdalevich, K. V. Grechnev, V. A. Ershova, V. G. Istomin, V. D. Ozerov, Ts. P. Dachev, I. S. Kutiev, T. N. Ivanova, J. Chereji, V. Mercea, D. Ristoiu, G. Toderjan, J. Rustenbach, J. Schmilauer

Introduction

Intercosmos-12 satellite was launched on October 31, 1974 with parameters: apogee — 718 km, perigee — 250 km, inclination — 74°. The main purpose of the experiment was to elaborate a measurement technique for charged particle density and ion mass composition of the ionospheric plasma. For that purpose, a mass-spectrometer and a set of probes for density and temperature measurements were mounted on board. That provided the possibility of comparing measurement results on ion composition between the mass-spectrometer and ion traps; on charged particle density between ion traps, Langmuir probe and radio-frequency capacity probe, and on the satellite potential-between all the instruments given above.

Unfortunately, because of technical reasons, both the ion traps and the Langmuir probe operated alternatively to the radio-frequency capacity probe.

This paper gives brief description on part of the above instruments and on some of the scientific problems which could be investigated by them.

The result processing is only in its initial phase, therefore here we would just compare results from mass-spectrometric measurements of ion composition to ion composition data obtained by simultaneous (or comparable) ion trap measurements. Such a comparison is important for the adjustment of the measurement results. Ion traps could give error in measurement of the main ion components (H^+ and O^+) because of small quantities of other ion components. On the other hand, the mass-spectrometer gives correct data only in a relatively small range of "attack angles", and the poor knowledge on the satellite orientation does not permit yet to obtain precise values both for absolute and for relative ion component densities.

Equipment

The radio-frequency mass-spectrometer was designed for measuring the ion composition as well as for elaboration of a measurement technique of neutral composition in upper terrestrial atmosphere. The radio-frequency mass-spectrometer (USSR and Czechosovakia) and the calibrator (Romania) were mounted on independent waterproof container with inner temperature and pressure control.

The calibrator was designed for the flight calibration of the mass-spectrometer in the measurement regime of neutral composition [1]. The calibrator originates a calibration flux of molecular hydrogen at the input of the mass-spectrometer. The principle of hydrogen diffusion through a thin wall of stainless steel at constant temperature is used.

The analyser A-2 of the MH-6407 P 2 equipment was used as sensor of the mass-spectrometer. The electronic device is more refined than that of MH-6407P and has the following specifics: resonant ions penetrating the collector are modulated in the section of the radio-frequency grids, which are supplied with amplitude-modulated high-frequency voltage. An a. c. amplifier with synchronous detector at the input effects the automatic scale selection dependent on the input signal voltage.

In all there are four scales with amplifying coefficient ratios of 1:10:100:1000. In real time telemetry regime the mass-numbers are measured in three subranges — 1-4 a. m. u.; 4-20 a. m. u.; 16-60 a. m. u. The recovery of these sectors provides a possibility for more precise discrimination within the accelerating potential in each of the sectors by the mutual control of the measurements at both ends of the subrange. In memory regime there are considerably narrower sectors of the range: about 1 a. m. u., about 4 a. m. u. and 14-18 a. m. u. The most important parameters — the frequency of the supplied voltage, its amplitude with respect to the retarding potential, the emission current of the ion source and some others become stable.

The Bulgarian-Soviet experiment of measuring positive ion density and electron density and temperature was performed with the help of theree-electrode spherical traps and Langmuir probe. Detailed equipment description has been given in [3].

In order to measure the electron density and the so-called "floating potential", a radio-frequency capacity probe was mounted on board, designed and made in the GDR [4]. This instrument measured the reactive impedance of a flat capacitor, immersed into the ionospheric plasma at a frequency of 10 MHz. The capacitor is a system of two disk grids 100 mm in diameter, fixed at 50 mm distance one from the other.

Results and Discussion

The volt-ampere characteristic of the spherical traps shows, as a rule, the availability of two ion components in ionospheric plasma at multiple orbital sectors (Fig. 1).

The analysis results for the case repetition frequency at a given difference of these components mass-numbers have shown that the maximal frequency of appearance of mass-numbers difference is about $M=14\div15$, which suggested that these components have to be considered as hydrogen ions (H^+, $M=1$) and oxygen ions (O^+, $M=16$). Based on that, the volt-ampere characteristic was effected under the consideration of the availability of these two ion species [5, 6].

On mass-spectrometric data, the information of reproduction seances Nos. 33, 77 and 78 (orbit 32, 76 and 77) was processed, as well as the direct emission of the 185th orbit for the following intervals: altitude — 500-710 km, geomagnetic latitude — ±50°, local time — 20:30-22:30.

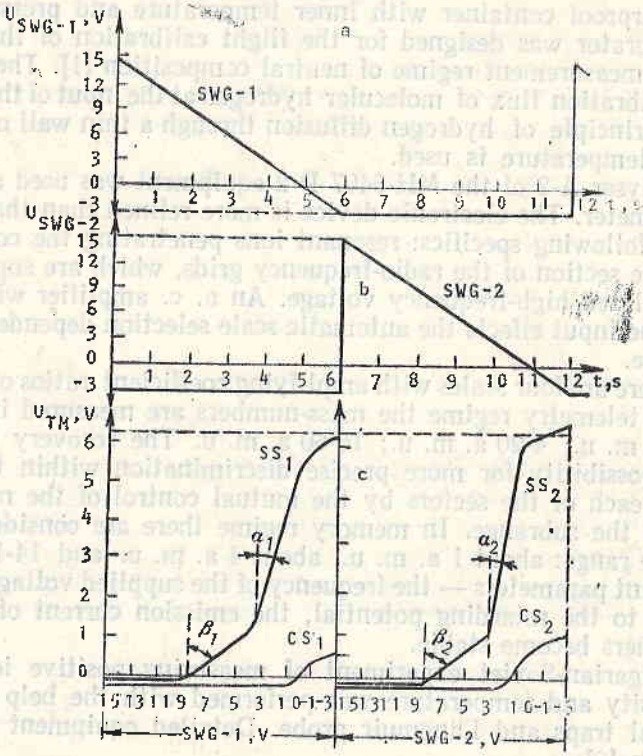

Fig. 1. Intercosmos-12: 34 orbit: H — 579 km, Φ — +14.5°, L — 1.14, A — 19°, LT — 21.37 h, λ — 134.6°

Table 1

Height, km	Geomagnetic latitude, deg.	Local time, hour min	Orbit	Mass spectrometer	Ion trap
711	—32	22 23	77	0.5—0.1	—
712	—29	22 27	76	0.5—0.1	0.2
711	—34		34		0.5
688	— 8	21 58	76	1—0.1	0.15
693	—21	22 41	32	1—0.1	
688	—13	21 57	77	1—0.2	
			34		0.4
638	11	21 34	76	2—0.4	0.72
553	34	20 58	76	2—0.4	0.72
560	20	21 30	34		2.0

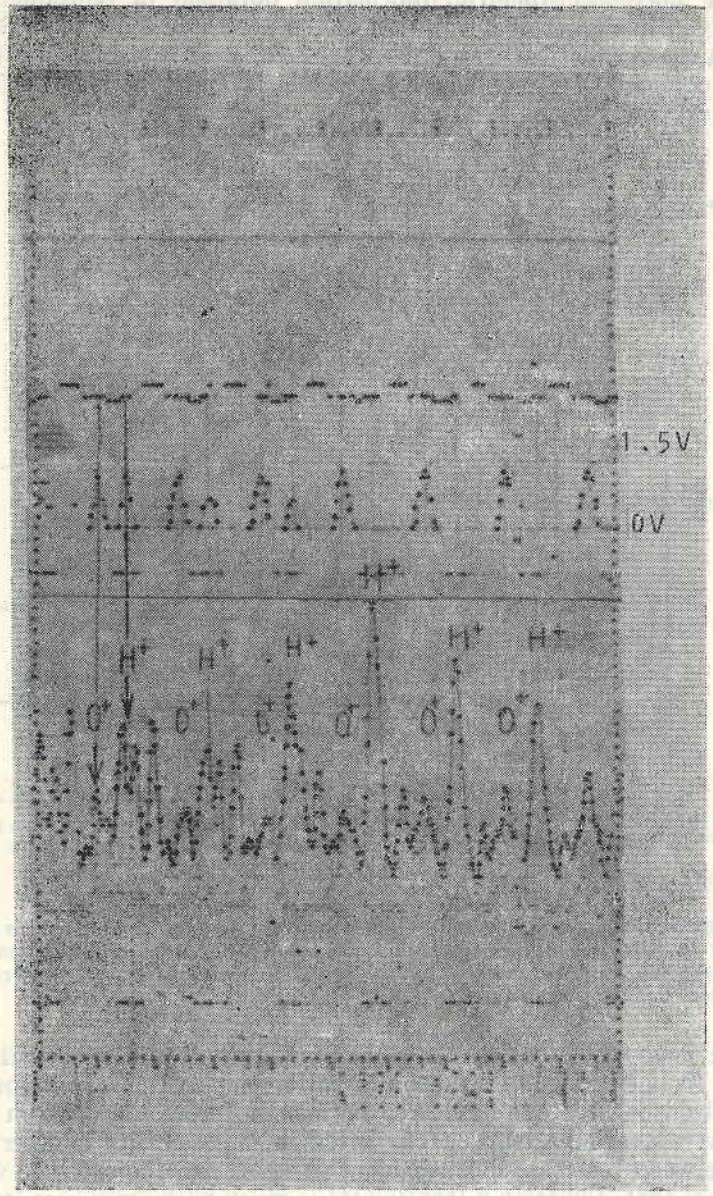

Fig. 2. Type of information obtained by mass spectrometer on board the Intercosmos-12 satellite. Data acquisition regime 77. SV — scanning voltage. The shape of the peaks determines the range of the mass (H+ or O+). IS — indication of sensitivity. The parameter is equal to: O volts at mass peaks below 6 V; 1.5 V — $<6\times10$V; 3V - $<6\times10^2$ V, 4.5 V — $<6\times10^3$ V. The SI impulses are distorted (real shape is rectangle) due to the small transmission band of the telemetry storage device. MS — mass spectrum. The measured peaks corresponding to the H+ and O+ ions are designated. The rest — peaks of the ions subject to registration during the reverse course of scanning and limited by the amplifier at the automatic switching of its dial

The mass-spectrometric information obtained in reproduction seance No. 77 is given in Fig. 2. The selection of the processed material was determined by the volume of spherical trap data processed by now (orbits 34, 76 and 185). The results compared between mass-spectrometric and spherical trap data are given in Table 1 and Fig. 3.

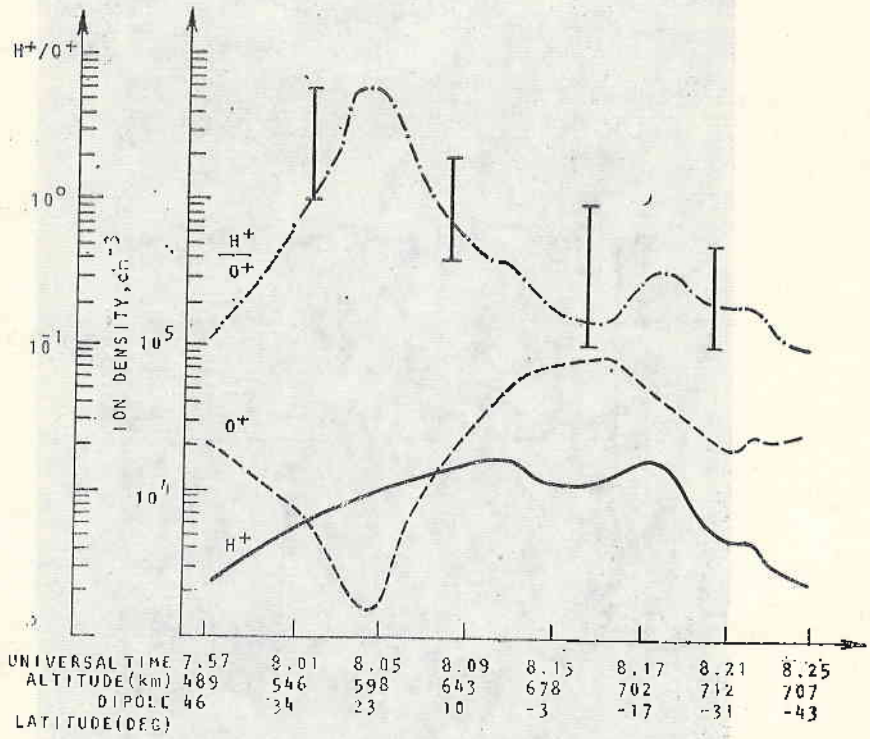

Fig. 3. Data about the ion composition obtained by traps and mass spectrometer in data acquisition regime 77 on the Intercosmos-12 artificial satellite. Traps, absolute ion concentration (solid and dashed lines). Traps, components ratio (dashed-dotted line)

The mass-spectrometric data have determined the ion density ratio n [H^+]/n[O^+]. As mentioned, the absolute calibration of mass-spectrometric data by the electron density was hampered because no processed data on satellite orientation were available, and that resulted in impossibility to determine the angle value between the mass-spectrometric analyzer and the satellite velocity vector. Because of that, the ratio n [H^+]/n[O^+] is given with error bars for the minimum angle of attack (evidently exceeding 0°). In order to evaluate these error bars the "angle characteristics" of O^+ and H^+ obtained for the analogous experiment Oreol-2 [7] have been used. The minimum attack angles were obviously located within the limits of 30-60°.

Certain indeterminateness of the ratio of ion densities, determined in memory regime, is introduced by the electronics specificity (the dynamic range of the equipment was not fully realized). In real time telemetry regime the picture was more positive, providing the fact that the results along the 185th orbit were from this disadvantage. Data on ion composition, obtained at the 185th orbit, were used for the specification of the minimum attack angle as well as the den-

sity ratio n $[H^+]/n[O^+]$. These specifications were effected with the help of data on the absolute density values of O^+ and H^+ by trap data. As already mentioned, the processing of trap data was carried out under the assumption of only two ion species being available. Nevertheless, the recording of He^+ by the mass-spectrometer and the data obtained on the relative He^+ density with respect to O^+ have permitted the correction of the results for the absolute ion density measured by the traps. At the 185th orbit on mass-spectrometric data, at minimum attack angles (maximum current for O^+), $n[H^+]/n[O^+]=0.9$. And on trap data, considering He^+, the same ratio is $5 \div 7$. (The interval is determined by the maximum scatter of the experimental points on trap data.) The discrepancy with the mass-spectrometric data from 6 to 8 times could obviously be explained with the discrimination of ions by the inlet angle, as the real attack angle is different from 0°. In order to explain such a discrepancy, we have to consider the value of the real attack angle being equal to 50-55° (by the angle characteristics used in [7]). The O^+ current reduced to 0° is of the order of $(4.8\text{-}6.6)\times10^{-11}$ a, which corresponds to $(1.4\text{-}1.6)\times10^4$ cm^{-3} by trap data. Therefore, the sensitivity of the mass-spectrometer with respect to O^+ ranges between 3 and 4×10^{-15} $A.cm^{-3}$.

Thus the value of the "angle characteristics" of the mass-spectrometer, together with the absolute ion density values obtained by the trap data, made it possible to effect absolute mass-spectrometric calibration by O^+ ions at definite orbital sectors. That gave the possibility to obtain rectified values of the ion density ratio H^+/O^+ at some of the other orbital sectors, by mass-spectrometric data (with no knowledge on the instrument tube orientation with respect to the satellite velocity vector) using only O^+ absolute density values obtained by the trap measurements.

Conclusion

As seen in Fig. 3 and Table 1, the nature of the relative H^+ density changes with respect to O^+ obtained by mass-spectrometric data agrees sufficiently with the probe measurements. The values of this ratio, measured by the traps, is within the limits of the interval determined by the mass-spectormeter.

References

1. Mercea, V., V. Istonin, J. Chereji, G. Todorean, D. Ristoiu. Calibrator for Space Flight Mass-Specrometer. — Rev. Roum. Phys., 8, 839, 1975.
2. Павленко, В. А., Б. Н. Зархин, А. Э. Рафальсон, М. Е. Слуцкий. — Космич. исслед., 4, 3, 457, 1966.
3. Chapkunov, S. K., T. N. Ivanova, M. Ch. Petrounova, K. B. Serafimov. Measurement of Electron and Ion Density and Temperature on the Intercosmos-12 Satellite. Paper B. 3. 11, XVIII Meeting of COSPAR, Varna, 1975.
4. Рустенбах, Ю., Д. Ломач. — В: ИНТЕРКОСМОС. Некоторые результаты научных экспериментов на ракетах „Вертикаль 1 и 2" и на спутниках „Интеркосмос 2 и 5". 150. Изд. АН ГДР, Институт электроники, ред. Ю. Рустенбах, К.-Х. Бишофф, Д. Фин, 1974.
5. Gdalevich, G. L. — Comt. rend. Acad. bulg. sci., 26, 755, 1973.
6. Гдалевич, Г. Л. — Изв. ГФИ, 20, 39, 1974.
7. Гречнев, К. В., В. А. Ершова, Ю. А. Шульчишин, Л. Д. Сивцева, С. В. Васюков, Ж. Кранье, Е. Блан, Ж.-А. Сово. Масс-спектрометрические измерения на спутнике „Ореол-2". — Космич. исслед. (в печати).

Анализ результатов масс-спектрометрических и зондовых измерений, проведенных на спутнике „Интеркосмос-12“

Г. Л. Гдалевич, К. В. Гречнев, В. А. Ершова, В. Г. Истомин, В. Д. Озеров, Ц. П. Дачев, И. С. Кутиев, Т. Н. Иванова, И. Кережи, В. Мерча, Д. Ристою, Г. Тодореян, Ю. Рустембах, Я. Шмилауер

(Р е з ю м е)

Спутник „Интеркосмос“ был выведен на орбиту 31 октября 1974 г. Параметры орбиты спутника: высота апогея 718 км, высота перигея 250 км, наклонение орбиты 74°. Основной задачей эксперимента была обработка методики измерений концентраций заряженных частиц и массового состава ионов в ионосферной плазме. С этой целью на спутнике была установлена масс-спектрометрическая аппаратура и комплекс зондов для измерения концентраций и температуры заряженных частиц. Благодаря этому оказалось возможным провести сравнение результатов измерений состава ионов, полученных с помощью масс-спектрометра и ионных ловушек, а также зонда Лэнгмюра и радиочастотного емкостного зонда, и потенциала спутника — посредством всех перечисленных приборов.

BULGARIAN ACADEMY OF SCIENCES

SPACE RESEARCH IN BULGARIA, 2

Sofia · 1979

Pulse Generator with Quartz Stabilization of the Frequency

B. P. Peev

Introduction

The large-scale application of integrated circuits in computing technology, in measurement equipment and in data processing systems has led to the solution of technical problems on a qualitatively higher level. In addition to the functions for which they are designed, the standard NAND gates can be interconnected to form various pulse generator circuits. In view of the requirements existing in the above fields as regards the stability and reliability of the pulse generators, increasingly frequent use has been made of circuits with highly stable delay lines or quartz resonators as time-setting elements.

This paper describes the operation and analyzes the characteristics of a pulse generator circuit with quartz stabilization of the frequency, which has been realized with standard two-input TTL NAND gates. The circuitry proposed avoids some of the shortcomings of the familiar circuitries (difficulties in the oscillations of the quartz resonator, oscillations of higher harmonics, and strong influence of variations in the supply voltage) and offers certain advantages (variable duty ratio of the output pulses, oscillation of the quartz resonator to the frequency of the serial resonance, and possibility of varying the frequency within narrow limits).

General Considerations Related to the Quartz Stabilization of the Pulse Generators

By the inclusion of a quartz resonator in the circuitry of the pulse generator, under thermostatic conditions of the resonator and of the electronic elements, it is possible to obtain instability of the frequency generated over a long period of time within the limits of 10^{-6} to 10^{-9} [2].

The equivalent electrical circuitry of the quartz resonator is approximately of the following type [2-4] — Fig. 1.

(1) $\omega_1 = \frac{1}{\sqrt{L_Q C_Q}}$ frequency of the serial resonance,

(2) $\omega_2 \cong \omega_1(1+0.5\ m)$ frequency of the parallel resonance,

(3) $m=\frac{C_Q}{C_0} \ll 1$ coefficient of incorporation of the quartz in the circuitry.

The circuitry proposed makes use of in-series control of the quartz crystal which is more efficient than the parallel one [3] and offers the following advantages:

— Lower tendency to parasitic oscillatons;

— Smaller change of the equivalent resistance controlling the generator upon deviation from the stabilized frequency;

— In-series control makes it possible to operate close to the frequency of the serial resonance.

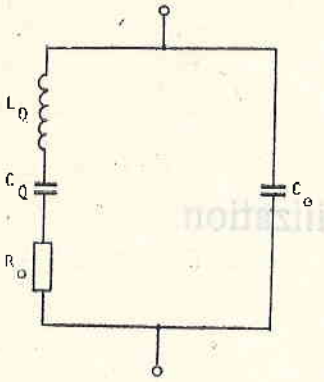

Fig. 1

L_Q — self-inductance of quartz; C_Q — self-capacitance of quartz; R_Q — resistance of quartz at t_Q; C_o — capacitance of quartz contacts

For the excitation of the quartz resonator in the circuitry of the pulse generator it must be connected between points in the circuitry which show great variation in the potential difference during operation [1, 2]. On the other hand, it is desirable for the quartz crystal to participate in the feedback circuit; this condition is not complied with in most practical circuits, but an additional condition is introduced, namely, that the period of the free oscillations generated (when the quartz resonator is not included in the circuitry) shall be 1.2 to 1.5 times smaller than the period of the stabilized oscillations [1, 3].

Operation of the Circuitry

On application of the supply voltage the circuitry begins generating free oscillations with a frequency $f_0=(1.2—1.5)\ f$, the quartz resonator playing the role of a capacitor. After about 100 ms [4] the resonator is excited and begins to oscil-

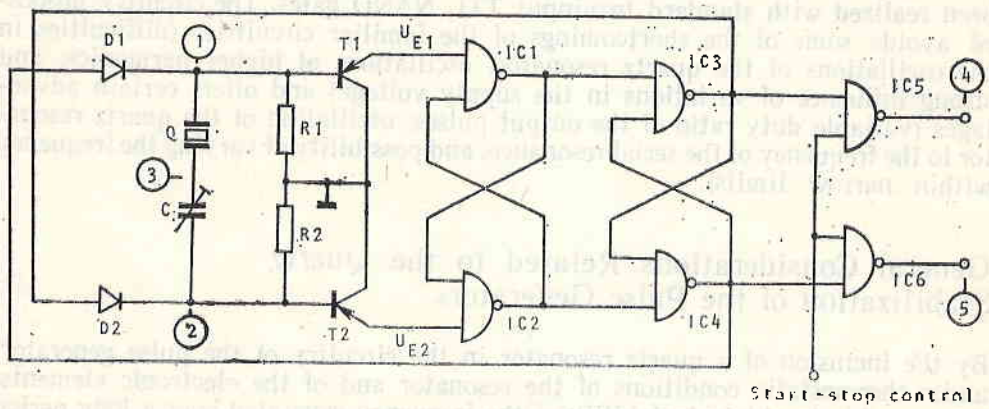

Fig. 2

late with a steadily growing amplitude. Upon reaching the rated amplitude of the oscillations, the pulse generator is synchronized with the frequency of the quartz resonator (Fig. 2).

Let us take the moment in which the voltage at point 1 of the circuitry changes with a jump from a "low" into a "high" level as the initial moment in the time-diagram. At the same moment the change of the voltage in point 2 is equal to the sum of the change in point 1 and the voltage applied on the quartz resonator.

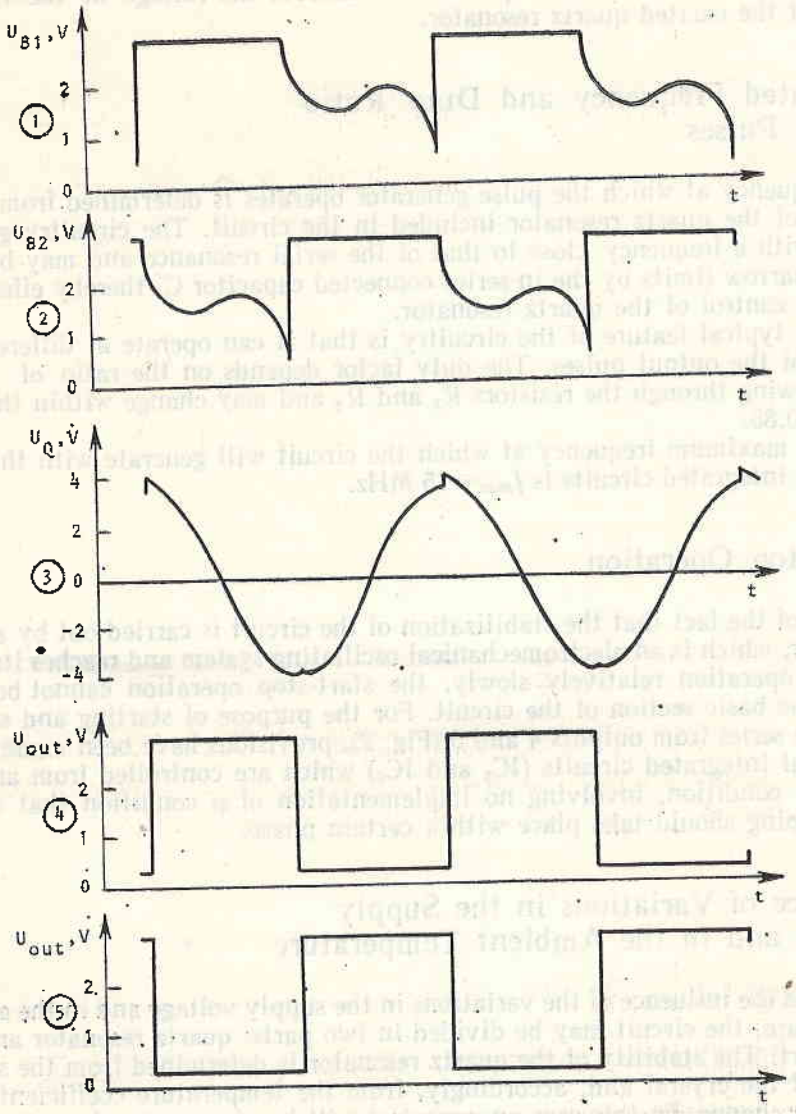

Fig. 3

The diode D_2 is reverse biased and is cut off, and the current of the excited quartz crystal begins to flow through the resistor R_2. At the moment when the voltage across the oscillating circuit (composed of the quartz crystal and of the in-series connected capacitor) becomes equal to 0, determined by the period of the series circuit, the current begins to flow in the opposite direction through the diode D_1 and the resistor R_2. Upon reaching the threshold level 0.8 V (U_E=1.5 V)

of the integtated circuit IC_1, the state of IC_1 and IC_2 (IC_3 and IC_4, respectively) changes and the voltage at point 2 changes with a jump to a "high" level. The process continues its development without stopping in the other branch of the system, the potentials at the respective points changing into the opposite ones. Figure 3 shows the voltages at typical points of the circuit, as a function of time. At point 3 of the circuit it is possible to observe the voltage of the first harmonic of the excited quartz resonator.

Generated Frequency and Duty Ratio of the Pulses

The frequency at which the pulse generator operates is determined from the frequency of the quartz resonator included in the circuit. The circuitry generates pulses with a frequency close to that of the serial resonance and may be varied within narrow limits by the in-series connected capacitor C, thereby effecting an in-series control of the quartz resonator.

One typical feature of the circuitry is that it can operate at different duty factors of the output pulses. The duty factor depends on the ratio of the currents flowing through the resistors R_1 and R_2 and may change within the limits of 0.15-0.85.

The maximum frequency at which the circuit will generate with the use of standard integrated circuits is $f_{max}=15$ MHz.

Start-Stop Operation

In view of the fact that the stabilization of the circuit is carried out by a quartz generator, which is an electromechanical oscillating system and reaches its steady state of operation relatively slowly, the start-stop operation cannot be realized in the basic section of the circuit. For the purpose of starting and stopping the pulse series from outputs 4 and 5 (Fig. 2), provisions have been made for two additional integrated circuits (IC_5 and IC_6) which are controlled from an external logic condition, involving no implementation of a condition that starting and stopping should take place with a certain phase.

Influence of Variations in the Supply Voltage and in the Ambient Temperature

As regards the influence of the variations in the supply voltage and in the ambient temperature, the circuit may be divided in two parts: quartz resonator and electronic part. The stability of the quartz resonator is determined from the selected section of the crysral and, accordingly, from the temperature coefficient of the frequency change. In this case an appraisal will be given only about the stability of the electronic part of the circuitry.

The summary influence of the changes in the supply voltage and in the ambient temperature (in the entire working range $U_c=+5$ V $\pm 5\%$, $T_a=0$—$70°C$) is expressed as instability of the frequency $\leqslant 10^{-7}$ (at a duty ratio for the output pulses $\delta=0.5$) [2] and tests of the circuitry under real conditions.

Practical Realization of the Circuitry of the Pulse Generator with Quartz Stabilization of the Frequency

Several variants have been realized of the examined circuitry, use being made of high-stability quartz resonators of the C. E. P. E. Company (Italy) and of the following electronic elements: SN74OON, SN74HOON, SN54OON, 1N914, 1N916, BAY71, BAY74, 2N2907, and BSX29. At a frequency of the quartz resonators 50 kHz and 100 kHz, of stabilized supply voltage and duty ratio of the pulses $\delta=0.5$, without taking any measures for temperature stabilization of the circuitry, an instability of 5×10^{-8} was measured for a period of 1 hour under laboratory conditions.

References

1. Пеев, Б. Импулсни генератори. - Трудове ЦИНТ, т. III, 1971.
2. Яковлев, В. П. Справочник по импульсной технике. Киев, 1970.
3. Альтшуллер, Г. Б. Кварцевая стабилизация частоты. М., 1974.
4. Львович, А. А., Ю. В. Гейсман. Высокостабильные кварцевые генераторы на туннельных диодах. М., 1970.
5. Изследване на спектрални характеристики на слънцето по време на слънчевото затъмнение 29. IV. 1976 г. ЦЛКН, БАН.
6. May, F. Multivibrator using IC. Electr. Appl., 29, 4, 1969.

Импулсный генератор с кварцевой стабилизацией частоты

Б. П. Пеев

(Резюме)

В связи с широким применением интегральных схем и требованиям к стабильности и надежности импульсных генераторов в системах обработки информации предлагается схема импульсного генератора с кварцевой стабилизацией частоты.

В работе описано действие и анализируются особенности предлагаемой схемы импульсного генератора. Данная схема лишена некоторых недостатков известных схем, а именно: отсутствуют трудности, связанные с возбуждением кварцевого резонатора, с возбуждением на высших гармониках и с влиянием напряжения питания. Показаны также преимущества данной схемы — переменный коэффициент заполнения выходных импульсов, возбуждение резонатора на частоте серийного резонанса, возможности изменения частоты в некоторых пределах.

Приводятся полученные результаты при практической реализации схемы импульсного генератора с кварцевой стабилизацией частоты.

ULGARIAN ACADEMY OF SCIENCES

PACE RESEARCH IN BULGARIA, 2

Sofia · 1979

Orbits of Artificial Earth Satellites Used in the Intersputnik System with Optimum Position for Bulgaria

P. Stoyanov, E. Alexandrova

This is an examination of the problems related to the determination of the optimum elliptic orbit for Bulgaria. Graphs have been given of geostationary and elliptic orbits with different longitudes of the apogee with respect to Sofia. The authors have analysed the conditions for communication of the other participants in the Intersputnik system when the satellite operates at an optimum orbit for our country. Quantitative evaluations have been given of the conditions for communication with an artificial earth satellite on elliptic and geostationary orbits.

Introduction

One of the forthcoming objectives of Bulgaria is the construction of an earth station (ES) for communications through artificial earth satellites (AES). In her capacity of participant in the Intersputnik international system for satellite communications, Bulgaria will operate with the satellites of that system and is interested in obtaining the optimum or near-optimum choice of the elliptic orbit to be used.

One basic variable parameter in the optimization of the conditions for operation with AES on an elliptic orbit is the position of the orbital plane in relation to Bulgaria. The distance between the meridian of the orbit apogee λ_A and the latitude λ_{ES} of the ES determines the proximity of the plane of the elliptic orbit.

The aim of our present work was to determine λ_A in such a manner as to obtain optimum conditions for communication between the AES and the ES of Bulgaria.

The optimum elliptic orbit is the one which ensures the following:

1. Maximum time for communication performance with AES;
2. Minimum in size biological zone of the ES;
3. Minimum by-pass angle in a horizontal direction.

This results in improvement of the electromagnetic compatibility with RRL operating or intended for operation in the band of joint operation with ES.

4. The noise temperature introduced through the aerial of the ES station from the atmosphere should be minimal.

Basic Dependences

The radius r_0 of the region of possible radio-communication between an ES and an AES travelling along an elliptic orbit of the Molniya-1 type is determined by the dependence (Fig. 1)

(1) $$r_0=\frac{\alpha_i}{180^0}\pi R,$$

where $2\alpha_i$ is an arc angle of the radiovisibility region from the satellite;

$i=1, 2, \ldots, n$ — points from the elliptic orbit; and R is the average Earth radius (6,370 km).

The angle γ characterizes the range of vision from an AES

(2) $$\gamma_i=\arcsin\frac{R\cos\beta_i}{R+H_{sat}}\text{ [grad]},$$

(3) $$\gamma_i\leq\Theta^{[\circ]}_{0.5p},$$

where $2\gamma_i$ is the span of the radiovisibility apex angle from an AES upon its travel along an elliptic orbit.

$2\Theta^{[\circ]}_{0.5p}$ is the width of the diagram of AES antenna oriented for operation at a half-power level. According to [1], $2\Theta^{[\circ]}_{0.5p}=20^\circ$.

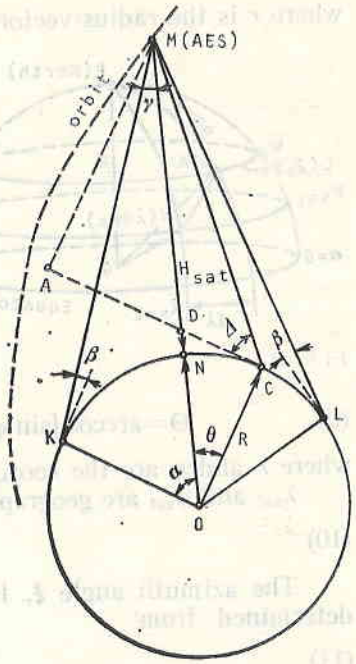

Fig. 1

(4) $$H_{sat}=r_i-R$$

is the height of the satellite above the Earth's surface; r_i — radius vector of an i point of the elliptic orbit where the satellite is to be found at the particular moment; and β_i is the minimum angle of operation of the aerial of the ES above the horizon.

In view of considerations for reducing the noise temperature of the aerial, as introduced from the Earth, $\beta_i\geq5^\circ$.

The dependence between the above angles is determined from

(5) $$\alpha_i=90^\circ(\gamma_i+\beta_i)\text{ [grad]}$$

and

(6) $$\beta_i=\arccos\frac{R+H^{sat}}{R}\sin\gamma\text{ [grad]}.$$

Determining the Optimum Elliptic Orbit for Bulgaria

The town of Sofia (geographic coordinates $\lambda=23^\circ$ e. l. and $\varphi=43^\circ$ n. l.) was selected as the observation point in determining the visibility of the satellite pass along a certain elliptic orbit. The position of the satellite in a vertical plane is

determined by the angle above the horizon Δ°, while the direction toward the horizon is determined by the azimuth angle ξ.

The angle Δ° is determined by the dependence

$$\Delta = \operatorname{arctg}\frac{AM}{CD+AD} = \operatorname{arctg}\frac{\cos\Theta - R/r}{\sin\Theta} \text{ [grad]}, \tag{7}$$

where r is the radius-vector of the point at which the AES is to be found, and Θ is the geocentric angle between the point of observation C (λ, φ) and the projection of the satellite on the Earth's surface N (λ_{sat}, φ_{sat}). The angle Θ determines the distance between the points C and N by the dependence

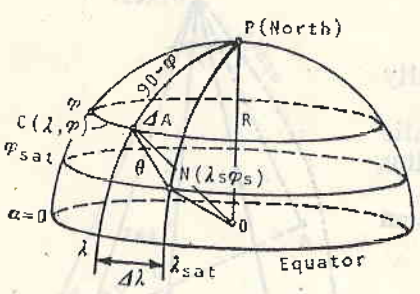

Fig. 2

$$Q = \frac{\Theta}{180^\circ} \cdot \pi R. \tag{8}$$

The angle Θ is determined from the spherical triangle NCP (Fig. 2)

$$\Theta = \arccos\left[\sin\varphi \cdot \sin\varphi_{sat} + \cos\varphi \cdot \cos\varphi_{sat} \cdot \cos\Delta\lambda\right] \text{ [grad]}, \tag{9}$$

where λ and φ are the coordinates of the observation point;

λ_{sat} and φ_{sat} are geographical coordinates of the satellite projection:

$$\Delta\lambda = \lambda_{sat} - \lambda. \tag{10}$$

The azimuth angle ξ, taken in a North-East — South-West direction, is determined from

$$\xi = \Delta A \tag{11}$$

when λ_{sat} is to the east of the meridian $\lambda = 23^\circ$ e. l. and from

$$\xi = 360^\circ - \Delta A \tag{12}$$

when λ_{sat} is to the West of the meridian $\lambda = 23^\circ$ e. l., while ΔA is determined from the spherical triangle NCP

$$\Delta A = \arccos\frac{\sin\varphi_{sat} - \sin\varphi \cdot \cos\Theta}{\sin\Theta \cdot \cos\varphi} \text{ [grad]}. \tag{13}$$

The geographic coordinates of the satellite λ_{sat}, φ_{sat} at any moment of its movement along the elliptic orbit are determined by the geocentric projection of the orbit on the Earth's surface. Figure 3 shows the geocentric projection of the odd elliptic trajectory, according to [2], due account being taken of the Earth's movement.

The projection of the even elliptic trajectory is a continuation of the odd one and has the position of the apogee λ''_A:

$$\lambda''_A = \lambda'_A + 180^\circ. \tag{14}$$

Figure 4 shows graphically presented elliptic orbits with different longitude of the apogee λ'_A (λ''_A), as they are seen from the selected observation point. The position of the satellite is determined in relation to the moment of time in which the AES passes through the perigee point ($t_o = 00$ h).

Table 1 gives the basic quantities which are characteristic of the elliptic orbit, namely: the radius-vector r, V^c (the angle between the direction to the perigee and r), the radiovisibility zone from the satellite (α, r_0) and the distance from the observation point to the projection of the satellite on the Earth's surface (Θ, ρ) for the selected elliptic orbits with different longitude of the apogee in function of absolute time.

For the purpose of determining the duration of the session for communication with the AES, we compare the visual zone of the AES from (1) and the distance to the undersatellite point from (8) (Table 1).

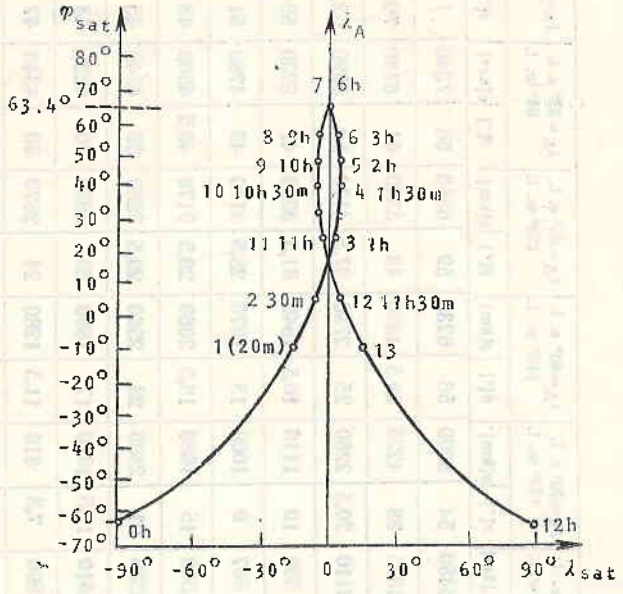

Fig. 3

1. At $\rho > r_0$ ($\Theta > \alpha$) the AES cannot "see" us with its aerials. Our visibility toward the satellite is determined by Δ from (7) and ξ from (11) or (12), and depends on the overlap angle to the horizon. When it is possible to ensure a minimum covering angle ($\beta_{min} = 5°$) for all orbits shown on Fig. 4, we can follow the movement of the satellite within an approximately 11-hour sector. In order to realize the communication session it is necessary to adjust the diagram of directed opetation of the satellite's aerial.

2. At $\rho \leqslant r_0$ ($\Theta \leqslant \alpha$) the AES satellite can be used to establish communication with member-country of the Intersputnik system. The boundary line $\rho = r_0$ at $\beta = 5°$ and $\gamma = 10°$, plotted by a broken line on Fig. 4, determines the duration of the communication session as shown in Table 2. The results obtained show that upon using one AES travelling along an elliptic orbit with different positions of the apogee, the total time of the communication session is a sum of two variable components.

The dimensions of the biological zone of the ES for protection from the irradiation of the aerial within the microwave band for persons not professionally involved in radiation and for the population is determined, as regards intensity, at 1 $\mu W/cm^2$ [3].

The size of the biozone depends on the power of the operating transmitters and on the values of the operative angles in horizontal and vertical directions. The dimensions of the biozones for the selected orbits at transmitter power $P_{tr} = 10$ kW, as well as the bypass angles from the aerial in a horizontal direction, are given in Table 2.

The noise temperature of the aerial T_{na} (introduced from dry atmosphere) is significant to the quality of the signal received from the satellite, whose value is of the order of 10^{-14} W/m^2. It depends on the angle above the horizon $\Delta°$ at which the aerial is operating

Table 1

No.	Time after the perigee, [h; min]	$V°$, [°]	$\bar{r}=R+H$ [km]	α [°]	$\bar{r}_0$ [km]	$\lambda_A=0°$ e. l. 180° w. l.		$\lambda_A=20°$ e. l. 160° w. l.		$\lambda_A=30°$ e. l. 150° w. l.		$\lambda_A=40°$ e. l. 140° w. l.		$\lambda_A=60°$ e. l. 120° w. l.		$\lambda_A=82°$ e. l. 98° w. l.		$\lambda_A=95°$ e. l. 85° w. l.		$\lambda_A=110°$ e. l. 70° w. l.	
						θ[°]	ϱ[km]	θ[°]	ϱ [km]	θ[°]	ϱ[km]	θ[°]	ϱ[km]	θ[°]	ϱ[km]	θ[°]	ϱ[km]	θ[°]	ϱ[km]	θ[°]	ϱ[km]
1	20 m	54,5	8376	3,2	350	63,1	7015	58	6450	54	6000	56	6230	59	6560	66	7340	/	/	/	/
2	30 m	76	9649	5,3	580	45,5	5058	39	4335	38	4225	39,5	4390	48	5340	61	6780	70	7780	/	/
3	1 h	117	18050	19,4	2153	26	2890	19	2110	20,5	2280	25	2780	37,5	4170	53	5890	62,5	6950	73	≥115
4	1 h 30 m	138	26573	36,4	4038	14	1560	5	556	10	1110	16,5	1840	31,5	3500	47	5230	56	6230	67	7450
5	2 h	149,5	33140	59,5	6615	15	1670	6	667	9	1000	15	1670	28,5	3170	43	4780	51	5670	59,5	6615
6	3 h	160,5	39387	76	8460	20	2220	14	1560	15	1680	18,5	2060	28,5	3170	40,5	4500	48	5340	55	6115
7	6 h	180	45961	77	8560	25	2780	21	2335	21	2335	23	2560	29,5	3280	39	4340	45	5010	51	5670
8	9 h	200,2	39103	76	8460	21,5	2390	14,5	1610	14,5	1610	17	1890	26	2890	38	4225	43	4780	53	5890
9	10 h	210	33324	59,5	6615	15,5	1720	8	890	7,3	810	11,5	1280	24	2670	39	4340	47	5230	56	6225
10	10 h 30 m	221,5	26811	37	4100	21	2330	8	890	5	556	10	1110	24,5	2720	40	4450	49	5460	59	6560
11	11 h	241	18680	20,5	2280	28,5	3170	20	2220	19,7	2190	27	2450	35	3890	50	5560	60	6680	70	7780
12	11 h 30 m	280	10615	6,1	750	41,5	4610	38	4225	39,5	4390	43	4780	53	5900	68	7560	71	7910	/	/
13	14 h	149,5	33140	59,5	6615	/	/	/	/	/	/	/	/	/	/	74	6230	68	7560	59,5	6615
14	15 h	160,5	39387	76	8150	79	8780	80,5	8950	80,3	89,30	79,3	8320	75,3	8370	68	7560	63	7000	54	6000
15	18 h	180	45961	77	8560	73	8115	74	8230	73,5	8170	73	8115	70	7780	64	7115	59,5	6610	54	6000
16	21 h	200,2	39103	76	8460	78	8670	80,4	8940	80,5	8950	80	8390	76,3	8480	70	7780	64,5	7170	58	6450
17	22 h	210	33324	59,5	6615	/	/	/	/	/	/	/	/	/	/	77	8660	71	7910	63	7000

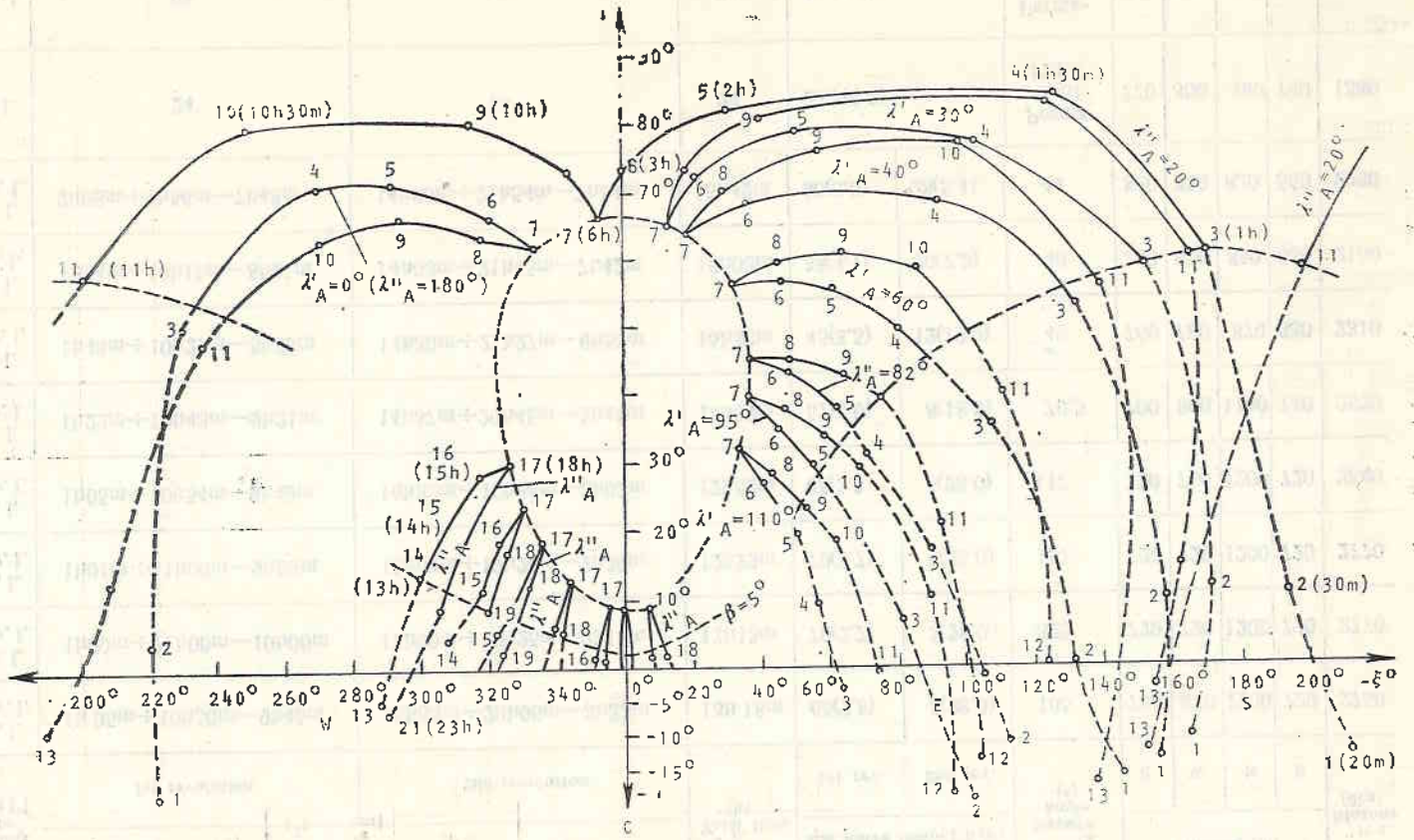
90°
80°
70°
30°
20°
-5°
-10°
-15°
0°
200°
220°
240°
260°
280°
300°
320°
340°
20°
40°
60°
80°
100°
120°
140°
160°
180°
W
S
E
-ξ°
9(10h)
10(10h30m)
5(2h)
4(1h30m)
6(3h)
7(6h)
3(1h)
2(30m)
1(20m)
21(23h)
λ'A=0°(λ''A=180°)
λ'A=30°
λ'A=40°
λ'A=60°
λ'A=95°
λ'A=110°
λ''A=82°
λ''A=20°
β=5°

Fig. 4

Table 2

No.	Longitude of the apogee [°]	Time of communication session: from -- to (h)		Total time (h)	Angle to the horizon and noise temp. [°]; [K]		Bypass angle [°]	Biozone [m]				Biozone (dca)
		1st revolution	2nd revolution		1st rev.	2nd rev.		E	W	N	S	
1	0° e. l. 180° w. l.	1h 05m÷10h50m—9h45m	16h33m÷20h06m—3h33m	13h 18m	65(2.8)	5(28.0)	105	760	670	1200	720	2750
2	20° e. l. 160° w. l.	1h00m÷11h00m—10h00m	17h00m÷19h25m—2h15m	12h15m	70(2.7)	5(28.0)	325	720	720	1200	720	2770
3	30° e. l. 150° w. l.	1h01m÷11h00m—9h59m	16h54m÷19h24m—2h30m	12h29m	70(2.7)	5(28.0)	151	720	720	1200	720	2770
4	40° e. l. 140° w. l.	1h05m÷10h54m—9h49m	16h32m÷19h36m—3h03m	12h52m	65(2.8)	5(28.0)	117	720	760	1200	720	2840
5	60° e. l. 120° w. l.	1h22m÷10h43m—9h21m	14h57m÷20h45m—5h48m	15h09m	57(3.0)	8(18.0)	70,5	700	800	1140	740	2820
6	82° e. l. 98° w. l.	1h48m÷10h27m—8h39m	14h30m÷21h27m—6h53m	15h32m	45(3.5)	12(12.0)	49	760	780	870	630	2310
7	96° e. l. 85° w. l.	1h54m÷10h15m—8h21m	14h03m÷21h45m—7h42m	16h03m	38(4.1)	20(7.3)	40	760	800	850	530	2150
8	110° e. l. 70° w. l.	2h08m÷9h56m—7h48m	14h00m÷21h54m—7h54m	15h42m	30(5.0)	28(5.4)	44	800	850	830	550	2280
9	68° e. l.	24	—	24	23.7(6.2)		Permanent 124.3°	770	350	490	740	1380
10	10° w. l.	24	—	24	30.1(5.0)		Permanent 223.6°	430	740	390	740	1320

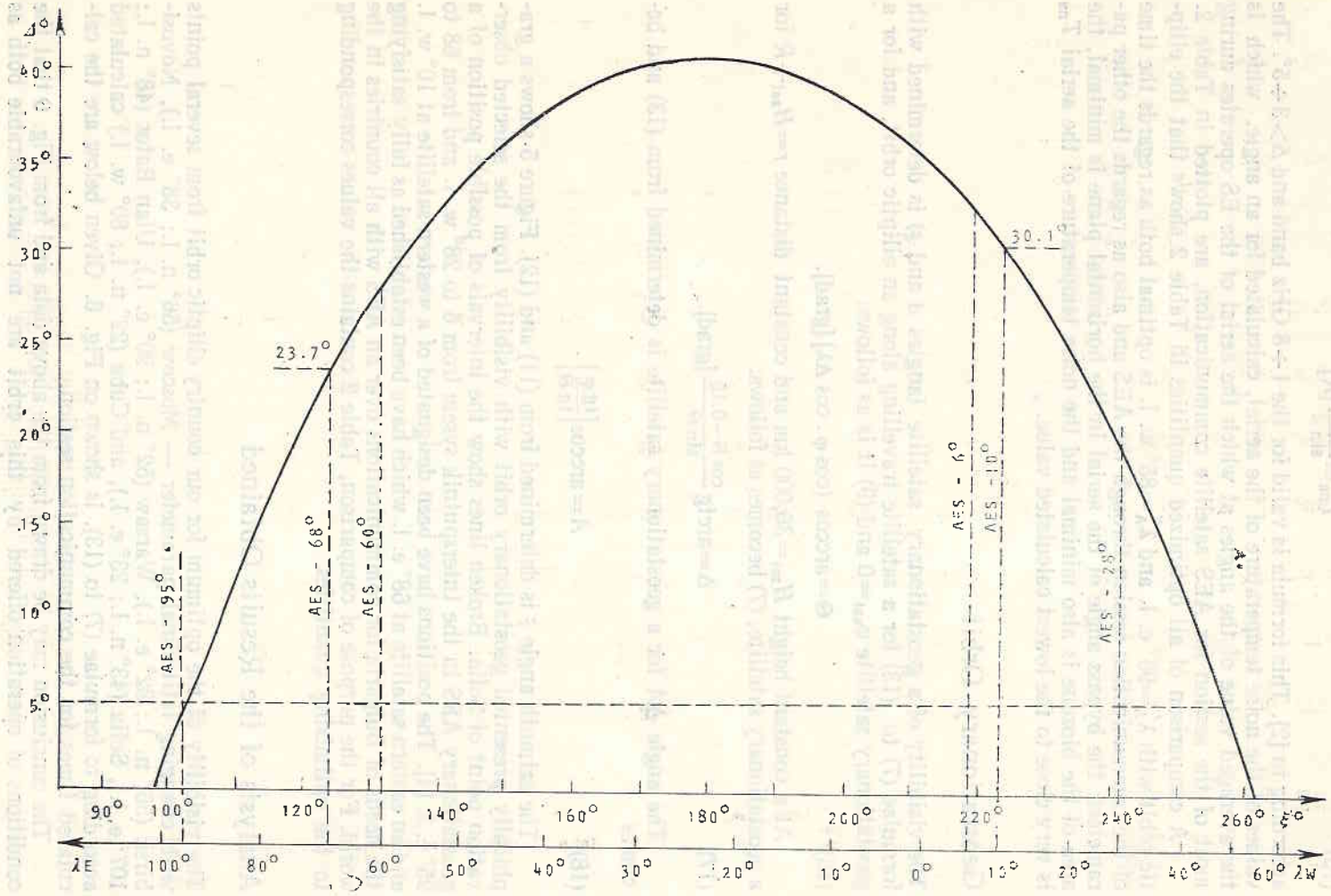

Fig. 5. Visibility of the geostationary orbit from Sofia ($\lambda = 23°$ e. l.; $\varphi = 43°$ n. l.)

(15) $$T_{na}=\frac{2.5}{\sin A}\ [K]$$

according to [2]. This formula is valid for the $1\div8$ GHz band and $\Delta>3\div5°$. The values of the noise temperature of the aerial, calculated for an angle, which is the averaged value of the angles at which the aerial of the ES operates during most of the session for AES satellite communication, are plotted in Table 2.

A comparison of all optimized quantities in Table 2 shows that the elliptic orbit with $\lambda'_A=95°$ e. l. and $\lambda''_A=85°$ w. l. is optimal both as regards the time of the communication session through the AES and also as regards the other parameters: the bypass angle of the aerial in the horizontal plane is minimal, the area of the biozone is also minimal and the noise temperature of the aerial T_{na} is very close to the lowest calculated value.

Geostationary Orbit

The visibility of a geostationary satellite (angles A and ξ) is determined with formulae (7) to (13) for a satellite travelling along an elliptic orbit, and for a geostationary satellite $\varphi_{sat}=0$ and (9) it is as follows:

(16) $$\Theta=\arccos\ (\cos\varphi\ .\ \cos\Delta\lambda]\ [\text{grad}].$$

At a constant height $H_{sat}=36{,}000$ km and constant distance $r=H_{sat}+R$ for a geostationary satellite, (7) becomes as follows:

(17) $$\Delta=\operatorname{arctg}\frac{\cos\Theta-0.15}{\sin\Theta}\ [\text{grad}].$$

The angle ΔA for a geostationary satellite is determined from (13) and becomes

(18) $$A=\arccos\left[\frac{\operatorname{tg}\varphi}{\operatorname{tg}\Theta}\right].$$

The azimuth angle ξ is determined from (11) and (12). Figure 5 shows a graphically presented geostationary orbit with visibility from the selected observation point of Sofia. Broken lines show the intervals of possible position of a geostationary AES in the Intersputnik sysem from 6 to 28° w. l. and from 68 to 95° e. l. [4]. The positions have been designated of a western satellite at 10° w. l. and an eastern satellite at 68° e. l. which have been established as fully satisfying the needs of Bulgaria for communications over an AES with all countries in the world. For the purpose of comparison, Table 2 contains the values corresponding to the optimizing quantities.

Analysis of the Results Obtained

The visibility of the optimum for our country elliptic orbit from several points with changing latitudinal parameter — Moscow (56° n. l.; 38° e. l.), Novosibirsk (55° n. l.; 82° e. l.), Warsaw (52° n. l.; 20° e. l.), Ulan Bator (48° n. l.; 107° e. l.), Sofia (43° n. l.; 23° e. l.), and Cuba (22° n. l.; 80° w. l.) calculated according to formulae (7) to (13), is shown on Fig. 6. Given below are the calculated times for the communication session.

The conclusion may be drawn from the above data and from Fig. 6 that the conditions of operation offered by this orbit are not unfavourable both as

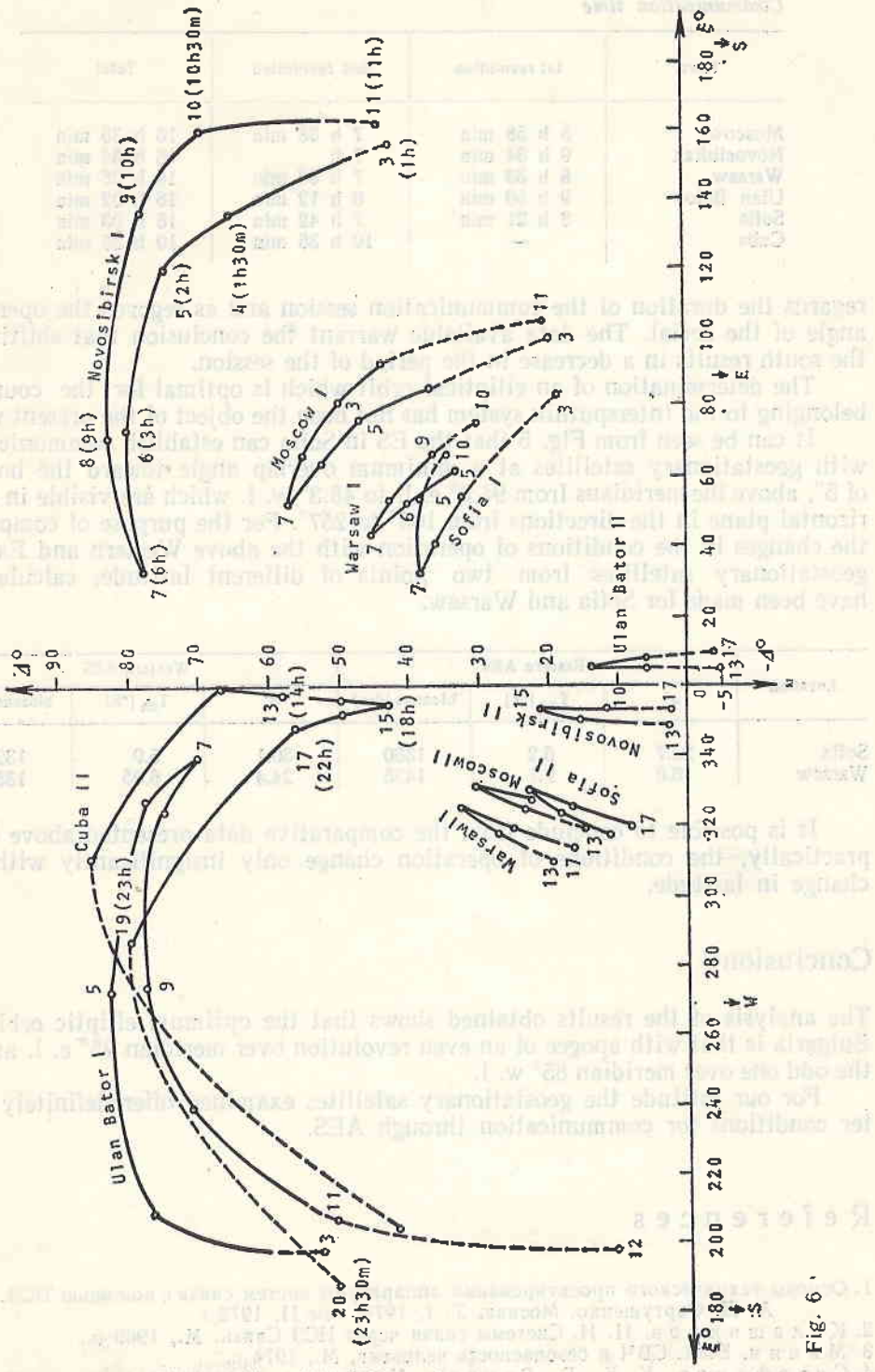
Novosibirsk I
Moscow I
Warsaw I
Sofia I
Ulan Bator II
Cuba II
Ulan Bator I
Novosibirsk II
Moscow II
Warsaw II
Sofia II
8(9h)
7(6h)
6(3h)
5(2h)
4(1h30m)
3(1h)
10(10h30m)
11(11h)
19(23h)
20(23h30m)
17(22h)
15(18h)
13(14h)
12
E°
W
S
N
Δ°

Fig. 6

Communication time

Town	1st revolution	2nd revolution	Total
Moscow	8 h 58 min	7 h 38 min	16 h 36 min
Novosibirsk	9 h 34 min	7 h	16 h 34 min
Warsaw	8 h 33 min	7 h 53 min	16 h 26 min
Ulan Bator	9 h 50 min	6 h 12 min	16 h 02 min
Sofia	8 h 21 min	7 h 42 min	16 h 03 min
Cuba	—	10 h 36 min	10 h 36 min

regards the duration of the communication session and as regards the operating angle of the aerial. The data available warrant the conclusion that shifting to the south results in a decrease in the period of the session.

The determination of an elliptical orbit which is optimal for the countries belonging to the Intersputnik system has not been the object of the present work.

It can be seen from Fig. 5 that the ES in Sofia can establish communication with geostationary satellites at a minimum overlap angle toward the horizon of 5°, above the meridians from 94.3° e. l. to 48.3° w. l. which are visible in a horizontal plane in the directions from 103° to 257°. For the purpose of comparing the changes in the conditions of operation with the above Western and Eastern geostationary satellites from two points of different latitude, calculations have been made for Sofia and Warsaw.

Location	Eastern AES			Western AES		
	$\Delta°$	T_{na} [°k]	biozone [dca]	$\Delta°$	T_{na} [°k]	biozone [dca]
Sofia	23.7	6.2	1380	30.1	5.0	1320
Warsaw	16.0	9.1	1425	24.4	6.05	1380

It is possible to conclude from the comparative data presented above that, practically, the conditions of operation change only insignificantly with the change in latitude.

Conclusion

The analysis of the results obtained shows that the optimum elliptic orbit for Bulgaria is that with apogee of an even revolution over meridian 95° e. l. and of the odd one over meridian 85° w. l.

For our latitude the geostationary satellites examined offer definitely better conditions for communication through AES.

References

1. Основы технического проектирования аппаратуры систем связи с помощью ИСЗ. Ред. А. Д. Фортушенко. Москва, Т. I, 1970; том II, 1972 г.
2. Калашников, Н. И. Системы связи через ИСЗ Связь. М., 1969 г.
3. Минин, Б. А. СВЧ и безопасность человека, М., 1974 г.
4. Серафимов, К. Б., Г. Гешчев. Космически радиоелектронни системи. София, 1973 г.

Оптимальные для НРБ орбиты ИСЗ, использованные в системе „Интерспутник“

П. Стоянов, Е. Александрова

(Р е з ю м е)

Рассмотрены вопросы, связанные с определением оптимальной для НРБ эллиптической орбиты. Графически представлены геостационарная и эллиптические орбиты с изменением географической долготы и апогея по отношению к Софии. Анализированы условия связи с другими участниками в системе „Интерспутник“ в условиях работы со спутником на оптимальной для нашей страны орбите. Даны количественные оценки условий связи со спутниками на эллиптических и геостационарной орбитах.

BULGARIAN ACADEMY OF SCIENCES

SPACE RESEARCH IN BULGARIA, 2

Sofia · 1979

Satellite Equipment for Determining the Overall Planetary Distribution of the Major Atmospheric Emissions — EMO-1

I. Purpose and Research Objectives, Measurement Technique, Optical Diagram and Mechanical Aspects

M. M. Gogoshev, S. K. Chapkunov, V. T. Simov, V. Vatsov, M. H. Petrounova, S. I. Surgoychev, Ts. N. Gogosheva, M. Vatsova, P. T. Petkov, N. P. Petkov

Purpose and Research Objectives

The interest shown in the study of the atmospheric emissions is due to the fact that they can be used in obtaining information on:

A. Important aeronomic processes in the ionosphere in the altitudinal range of 60 to several thousand kilometers above the Earth's surface. Significant among these processes are the dissociative recombination of the molecular ions in the E and F ionospheric regions, a large spectrum of ion-exchange reactions, and the radiative recombination.

B. The precipitation of protons and electrons of different energy.

C. The heating of the high atmosphere under the effect of electromagnetic waves of various nature and genesis, and also the detecting of acoustic and inner gravitational waves.

D. The ionospheric-magnetospheric interactions.

E. The study of various aspects of the physics of solar-terrestrial relationships.

Measurements of the spectrum of the luminescent atmospheric layers are usually carried out from observation points fixed on the Earth's surface. This method offers certain advantages (possibility for continuous observations, continuity and homogeneity of the data, etc.), but it has a number of disadvantages as well. In the first place, we would like to refer to the spatial limitations of the data obtained. By way of example we would like to take the case of the magnetospheric-ionospheric interaction. The penetration of energy from the magnetosphere to the ionosphere is not the same at different points of the Earth's surface. This is due to the sectoral structure of the magnetosphere which is related not only to the shape of the terrestrial magnetic field but also to the diur-

nal rotation of the Earth, to the constant change in the direction to the Sun, for any given point. Consequently, it is not possible to obtain sufficiently complete information for this effect from such a fixed point. The network of observation stations is most unevenly distributed, and observations are often unavail-

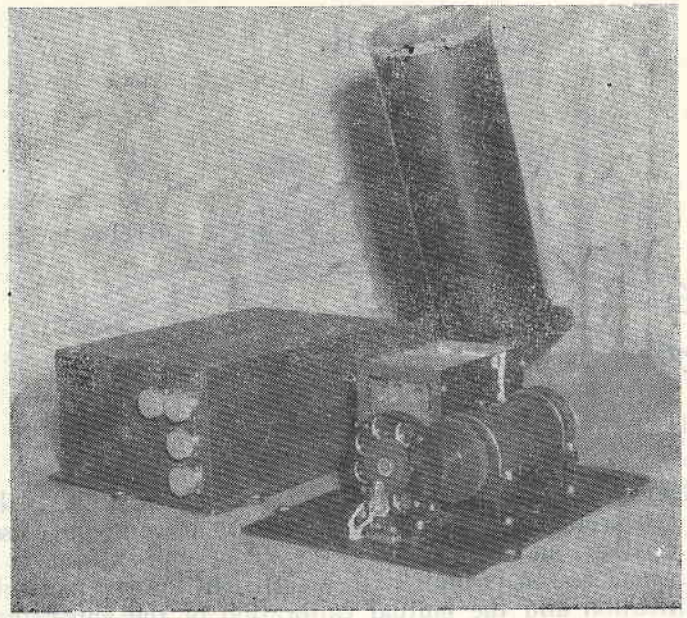

Fig. 1

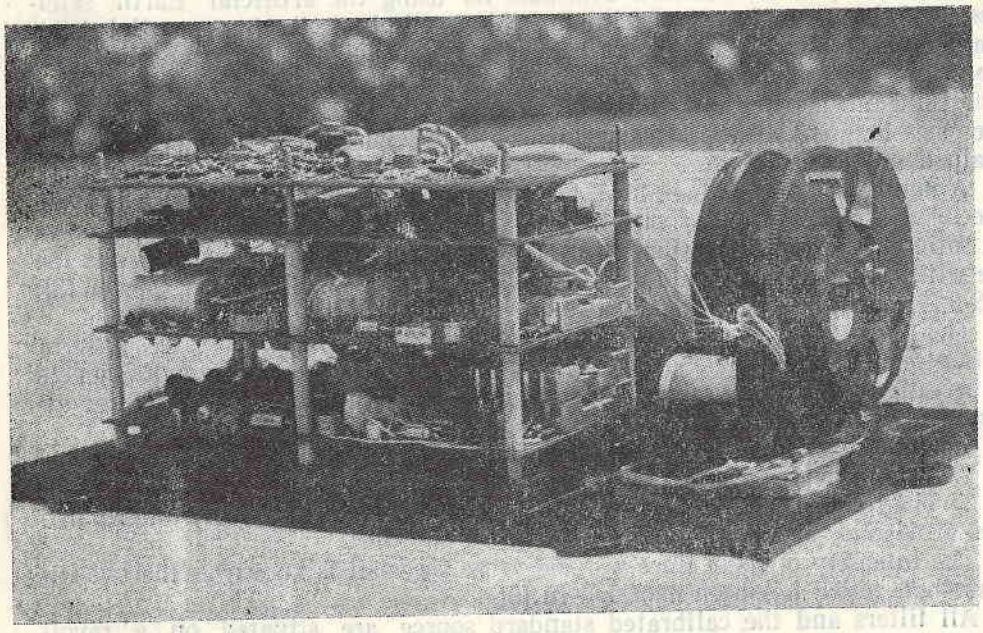

Fig. 2

able where they are most needed, e. g. in the region of the polar casp, in the mid-latitudinal trough, and in the crests of the geomagnetic equatorial anomaly. On the other hand, even if there was a sufficiently complete network of observation stations, their data would not have been sufficient to carry out magneto-

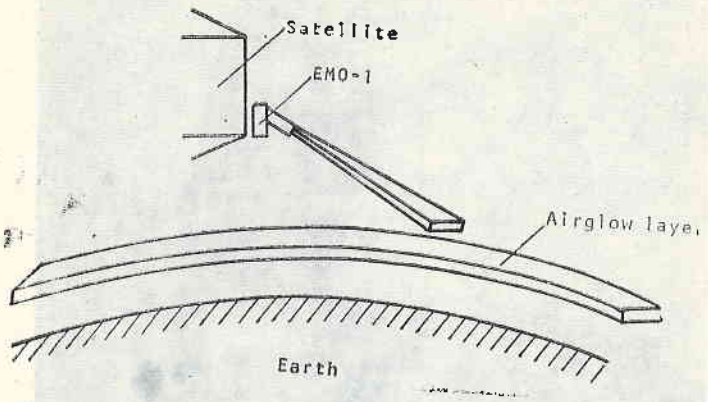

Fig. 3

spheric investigations for the following two reasons: The first one is that in view of the need of synchronization, it becomes necessary to carry out observtions at periods of bad weather, in the presence of the Moon, etc., and this is not always possible. The second reason is that, with a sufficiently large network of observation the unification and the mutual calibration of the apparatuses used is practically impossible. This, of course, will lead to essential differences and to incompatibility of the data obtained.

With the possibilities now available for using the artificial Earth satellites (AES) for research purposes, it is possible to eliminate the two essential shortcomings of the terrestrial apparatuses. By the satellite electrophotometers it is possible to obtain overall planetary characteristics of the atmospheric emissions. And in view of the fact that these apparatuses fly in a complex set with other measurement devices, the scientific justification and the value of the data obtained are much greater.

A number of apparatuses have been developed in the course of the last decade for operation on board various satellites, whose aim is the investigation of the optic atmospheric emissions in a broad spectral and energy range, as is the case with the equipment on board the OGO-4 [1, 2], Atmospheric Explorer [3], ISIS-2 [4, 5] and many other satellites.

The present article describes the electrophotometric apparatuses designed at the Central Laboratory for Space Research of the Bulgarian Academy of Sciences for investigating the overall planetary distribution of the following major atmospheric emissions:

1. The red oxygen double OI ($^3P—^1D$)λ 6300—6364 Å.
2. The green oxygen line OI ($^1D—^1S$)λ 5577 Å.
3. The line λ 4278 Å from the first negative system of the singly-ionized nitrogen molecule.

The intensity of these lines was measured by what is known as the two-filter method which has been explaied in [6].

All filters and the calibrated standard source are situated on a revolving disk.

A general view of the photometer is shown on Fig. 1. Figure 2 shows individual units of the equipment. Figure 3 presents the measurement diagram, realized by means of a satellite with a minimum altitude of 500 km, which is oriented and stabilized with respect to the Earth's surface. The electrophotometer EMO-1 is fitted to the board side and is oriented at a given angle to the Earth's surface ($\gamma=79°$). An analogous diagram is to be found, by way of example, in OGO-6 [7].

The angle γ is selected in accordance with the following considerations. At a minimum altitude of the satellite of 500 km, the optic axis of the photometer must be tangential to the Earth's surface. At the passage to the perigee altitude, and at the perigee, the photometer measures emissions from different atmospheric layers at a certain altitide above the Earth.

Optical Diagram

The selection of the optical diagram is determined by the orbital parameters, by the altitudinal dimensions and the distribution of the emitting layers, and by a certain destabilization of the carrier. In accordance with the above considerations, a rectangular field of vision has been selected with vertical dimension 1° and horizontal dimension 3.5°. The photo receiver was FEU-79 whose spectral curve embraces the range examined with very high sensitivity.

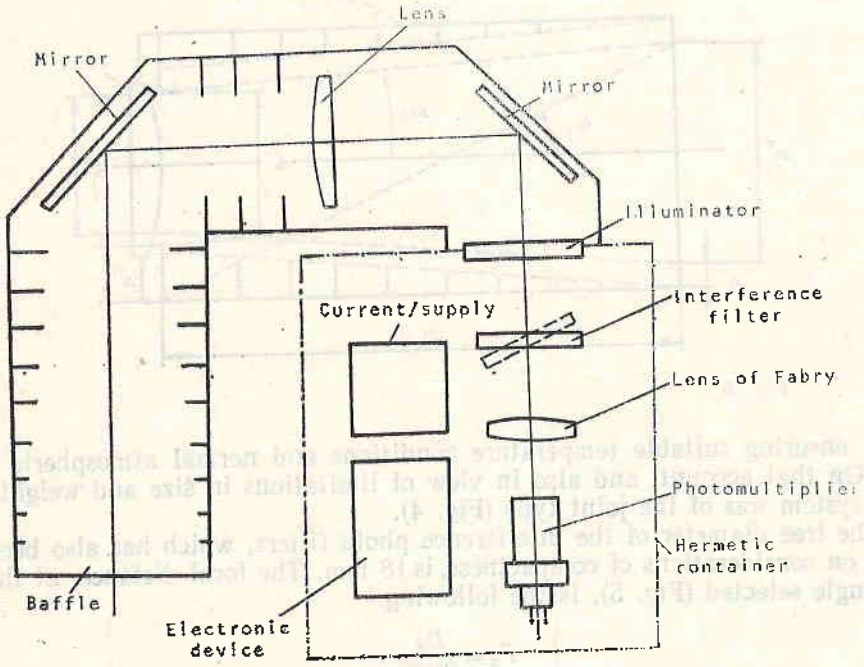

Fig. 4

The principal function of the optical diagram in this case is to improve the signal-to-noise ratio and also to locate the emitting layers. In selecting this system it is sometimes necessary to take account of incompatible and contradictory requirements related to the weight of the device, its size, and its structural and technological requirements. A two-component Keplerian telescopic system

has been selected in this case. In order to reduce the weight and to minimize the losses of absorption, two simple lenses were selected for objective and ocular (Fabri's lens).

To ensure the correct operation of the interferential photo filters, the photoelectric multiplier, together with the electron blocks, is placed in a sealed con-

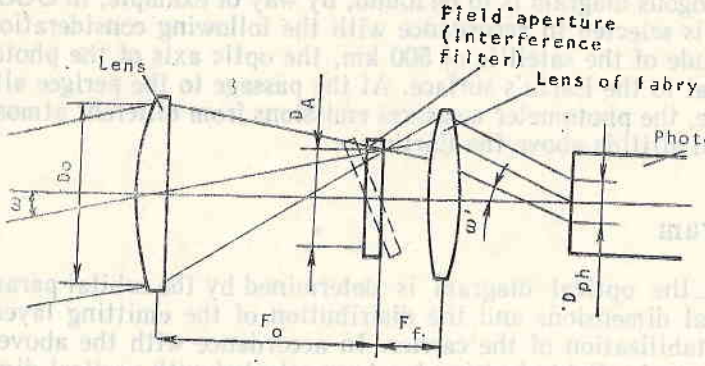

Fig. 3

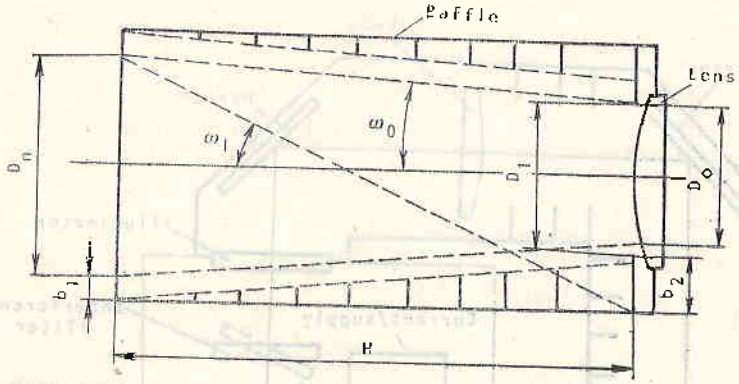

Fig. 5

tainer ensuring suitable temperature conditions and normal atmospheric pressure. On that account, and also in view of limitations in size and weight, the optic system was of the joint type (Fig. 4).

The free diameter of the interference photo filters, which has also been selected on considerations of compactness, is 18 mm. The focal distance, at the visual angle selected (Fig. 5), is the following:

$$F_0 = \frac{D_d}{2\operatorname{tg} W_0}, \tag{1}$$

where F_0 is the focal distance of the objective, D_d is the size of the blind of the visual field, and W_0 is one-half the angle of the visual field. In this case, at a visual angle of 3.5°, the focal distance of the objective is 284.2 mm.

The basic ratio for the telescopic systems is

$$\gamma_0 = \frac{F_0}{F_{if}} = \frac{D_0}{D_0'}, \tag{2}$$

where F_{lf} is the focal distance of the ocular (Fabri's lens), D_0 is the diameter of the input aperture (coinciding with the diameter of the objective), and D_0' is the diameter of the ou put aperture.

With a view to the optimum utilization of the optic system as a transmitter of photoenergy, it is necessary for the photocathode of FEU to be in the plane of the output aperture. Besides that, the output aperture must be equal to or smaller than the diameter of the photocathode. Then it follows from (2) that at a 60 mm diameter of the objective we shall have

$$\gamma_0 = 10 \text{ and } F_{lf} = 24.42 \text{ mm}. \tag{3}$$

The operation of the apparatus is accompanied by the influence of strong sources of light situated close (at an angle) to the regions subject to measurement. These sources usually have radiation energy (their own or reflected) exceeding the energy measured. The tube with protective diaphragms (Fig. 6) is used to eliminate the influence of these sources. The principal dimensions of this system are determined from the following formulae

$$D_1 = \frac{D_0}{\operatorname{tg} W_1 - \operatorname{tg} W_0}, \tag{4}$$

where D_0 is the free diameter of the objective, W_1 is the angle of the protection, and W_0 is one-half the angle of the visual field.

$$H_{\min} = \frac{(D_1 + B_2)\cos(W_1 + \Delta W_1)\cos W_0}{\sin[(W_1 + W_1) - W_0]}, \tag{5}$$

where B_2 is the depth of the blind and ΔW_1 is the angle of deflection of the axis of the apparatus from its nominal position as a result of the incomplete stabilization of the object.

$$D_p = D_0 \frac{\operatorname{tg} W_1 + \operatorname{tg} W_0}{\operatorname{tg} W_1 - \operatorname{tg} W_0}. \tag{6}$$

In this formula D_0 is the diameter of the last diaphragm.

All diaphragms have sharp edges and curvature radius not exceeding several microns. In order to reduce the background noise from the edges, only the first and the last diaphragm are situated outside, parallel to it at a distance B_1.

The position of the diaphragms along the axis has been determined graphically. In order to reduce the amount of the dispersed light, the inside of the tube is furrowed and light-absorbing coatings are laid on the polished diaphragms.

To reduce the dispersed light in the optical glass, the latter has been selected with minimum bubbles and non-uniformities in its structure.

We know that under conditions of radiation the optic glasses reduce their transparency coefficient and become stained. This leads to errors in measurement. Special types of glass have been selected in order to avoid this shortcoming, and their properties are not affected by the radiation.

Mechanical Equipment

The body of the EMO-1 device consists of the following principal units (Fig.7): base (1), cover (3) and tube with protective diaphragms (2). Fitted to the base are the unit with FEU, the electronic block, the disk with the filters, and the step-by-step generator.

This design provides for easy assembly and adjustment of the device, since free access is obtained to the basic unit by the removal of the cover. The base

has six apertures by means of which the device is attached to the carrier, thereby providing for efficient heat exchange. The cover (3) ends in a flange whose groove contains vacuum rubber 4 mm thick. The casing of the optic system is fitted to the front part of the cover. The latter ends with a socket in which the tubes with

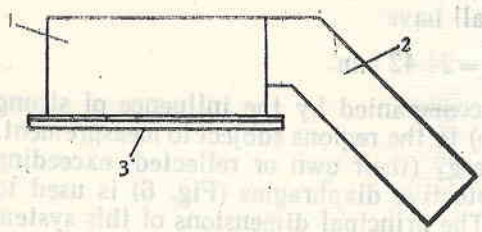

Fig. 7

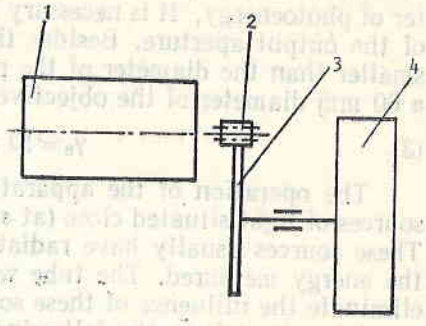

Fig. 8

the optic elements are secured. Further fitted to the cover are an illumination admitting the photo flux to the sealed part of the device, four sealed connectors and a pipe connection for filling the device with inert gas.

Kinematic Diagram

In selecting the kinematic diagram the aim is to perform the cyclic rotation of the disk with the interference photofilters by a minimum number of elements. Out of the possible solutions — ratchet gear, Geneva wheel, driving with single-revolution clutch, and step-by-step motor, the choice fell on the last one. Fig. 8 shows the kinematic diagram of the drive. The step-by-step motor with bipolar control has the following characteristics: supply voltage 15 V, power 1.5 W, and weight 0.7 N. The control of the motor is shown on the block diagram shown on Fig. 9, in which PG is a generator of tact pulses, CR is a resolution circuit, PM is a prohibiting monovibrator, ID is a pulse distribution, PA is a power amplifier, and M is a step-by-step motor.

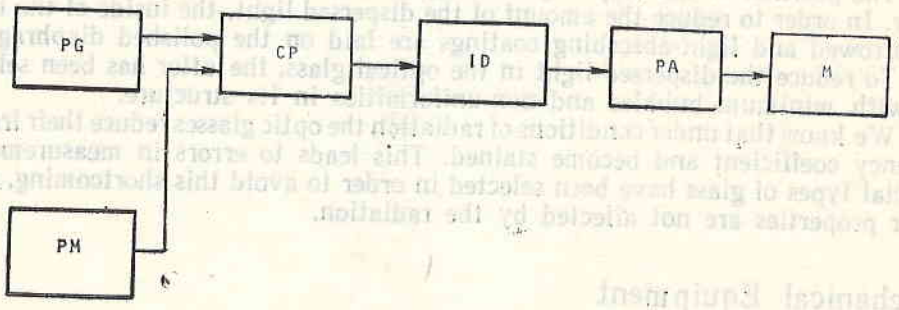

Fig. 9

The pulse generator provides rectangular pulses with a period $T=200$ ms. These pulses are sent to the pulse distributor while there is no ban from PM. The prohibiting pulse from PM has a duration of 1.2 sec. The pulse distributor ID converts the pulses received into a two-phase system (Fig. 10), phases A and B.

These rectangular pulses from the power amplifier are fed to the step-by-step motor M. Integrated logic circuits have been used in the design of PG, PM, ID and CP.

The power amplifier PA is of the non-reversive type and is fed by a d. c. supply. PA consists of two identical channels amplifying the ID pulses obtai-n

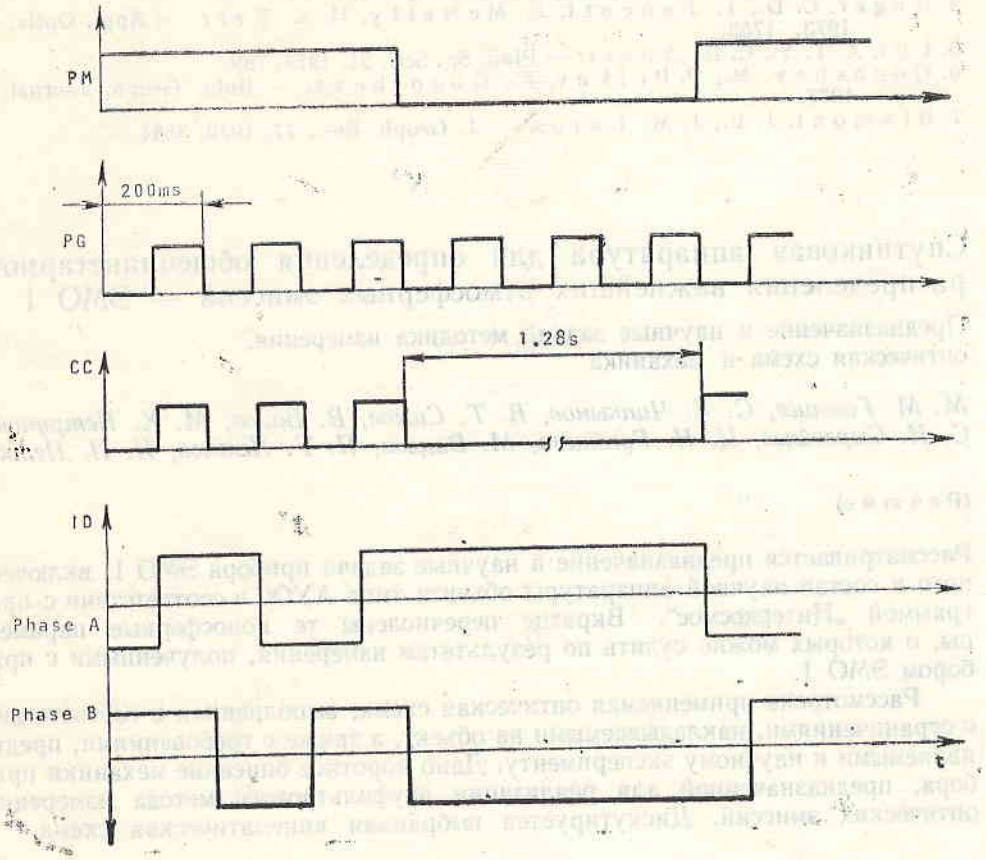

Fig. 10

ed. The PA amplifier is designed with silicon transistors operating on a key pattern.

The step-by-step motor, according to the block diagram on Fig. 10, will move until it receives a prohibiting impulse from PM. Upon reaching a particular position, the motor and the disk with filters connected to its axle stop for a certain time, during which a measurement is taken. After that the motor is reset. The eight positions of the disk are covered successively in this manner.

When two of the authors (M. G.and Ts. G.) first suggested the idea of using these apparatuses, it obtained full support and its realization became possible thanks to the active assistance of Professor K. Serafimov, Corresponding Member of the Bulgarian Academy of Sciences and Director of the Central Laboratory for Space Research in Sofia. The authors would like to express their warmest gratitude to him.

References

1. Reed, E. L., W. B. Fowler, J. E. Blamont. — J. Geoph. Res., 78, 1973, 5658.
2. Hicks, G. T., T. A. Chubb. — J. Geoph. Res., 75, 1970, 6233.
3. Hays, P. B., G. Garignan, B. C. Kennedy, G. G. Shepherd, J. C. G. Walker. — Radio Science, 8, 1973, 369.
4. Anger, C. D., T. Fancott, J. McNally, H. S. Kerr. — Appl. Optic, 12, 1973, 1753.
5. Lui, A. T. Y., C. D. Anger. — Plan. Sp. Sci., 21, 1973, 799.
6. Gogoshev, M., P. Petkov, Ts. Gogosheva. — Bulg. Geoph. Journal, 3, 1977.
7. Blamont, J. E., J. M. Luton. — J. Geoph. Res., 77, 1972, 3534.

Спутниковая аппаратура для определения общепланетарного распределения важнейших атмосферных эмиссий — ЭМО 1

Предназначение и научные задачи, методика измерения, оптическая схема и механика

М. М. Гогошев, С. К. Чапкынов, В. Т. Симов, В. Вацов, М. Х. Петрунова, С. И. Сыргойчев, Ц. Н. Гогошева, М. Вацова, П. Т. Петков, Н. П. Петков

(Резюме)

Рассматривается предназначение и научные задачи прибора ЭМО 1, включенного в состав научной аппаратуры объекта типа АУОС в соответствии с программой „Интеркосмос". Вкратце перечислены те ионосферные параметры, о которых можно судить по результатам измерения, полученными с прибором ЭМО 1.

Рассмотрена применяемая оптическая схема, выполненная в соответствии с ограничениями, накладываемыми на объект, а также с требованиями, предъявляемыми к научному эксперименту. Дано короткое описание механики прибора, предназначенной для реализации двуфильтрового метода измерения оптических эмиссий. Дискутируется выбранная кинематическая схема.